3-23-2018

Analysis of Temperature and Humidity Effects on Horizontal Photovoltaic Panels

Corey J. Booker

ANALYSIS OF TEMPERATURE AND HUMIDITY EFFECTS ON HORIZONTAL PHOTOVOLTAIC PANELS

THESIS

Corey J. Booker, Capt, USAF

AFIT-ENV-MS-18-M-180

DEPARTMENT OF THE AIR FORCE
AIR UNIVERSITY

AIR FORCE INSTITUTE OF TECHNOLOGY

Wright-Patterson Air Force Base, Ohio

AFIT-ENV-MS-18-M-180

ANALYSIS OF TEMPERATURE AND HUMIDITY EFFECTS ON HORIZONTAL PHOTOVOLTAIC PANELS

THESIS

Presented to the Faculty

Department of Engineering Management

Graduate School of Engineering and Management

Air Force Institute of Technology

Air University

Air Education and Training Command

In Partial Fulfillment of the Requirements for the

Degree of Master of Science in Engineering Management

Corey J. Booker

Captain, USAF

23 Feb 2018

AFIT-ENV-MS-18-M-180

ANALYSIS OF TEMPERATURE AND HUMIDITY EFFECTS ON HORIZONTAL PHOTOVOLTAIC PANELS

Corey J. Booker

Captain, USAF

Committee Membership:

Alfred E. Thal, Jr., PhD
Chair

Diedrich Prigge V, PhD
Member

Brent T. Langhals, PhD
Member

Lt Col Torrey J. Wagner, PhD
Member

Abstract

The United States Air Force seeks to address power grid vulnerability and bolster energy resilience through the use of renewable energy sources. Air Force Institute of Technology engineers designed and manufactured control systems to monitor power production from the most widely-used silicon-based solar cells at 38 testing locations around the globe spanning the majority of climate types. Researchers conducted multivariate regression analysis to establish a statistical relationship between photovoltaic power output, ambient temperature, and humidity pertaining to monocrystalline and polycrystalline photovoltaic panels. Formulated models first characterized power output globally, then by specific climate type with general inaccuracy. Location-specific models are provided with varying accuracy, allowing a number of locations to predict energy output and make decisions regarding future energy projects. It was found that additional predictor variables are required to hone model accuracy. Recommendations are made that modify the current study for the purpose of increasing data quality as well as ensuring the validity and accuracy of resulting regression models and the future ability to forecast power production for use by decision-making authorities. Further, a full year of measurements combined with proposed modifications will demonstrate feasibility of utilizing horizontal photovoltaic technology.

Table of Contents

Page

List of Figures

Page

List of Tables

Page

ANALYSIS OF TEMPERATURE AND HUMIDITY EFFECTS ON HORIZONTAL PHOTOVOLTAIC PANELS

I. INTRODUCTION

Energy resilience is a global issue and an especially key concern for the United States Air Force. Meeting energy needs through practical and regulatory requirements will necessitate exploration of renewable technologies. One such technology is photovoltaic (PV) panels, commonly referred to as solar panels, which convert solar irradiance into usable electricity. This research builds upon a prior feasibility study on the use of PV pavement technology and will test its underlying principle: horizontal placement of silicon-based PV panels to capture direct and diffuse radiation. To accomplish this, power output must be measured in various climate types around the world having broad temperature and humidity ranges for a sufficient period of time. This will allow researchers to observe and record relationships between environmental factors affecting panel performance.

General Issue and Background

Securing energy resources for the purpose of national security is a primary focus for United States military and political leadership. The National Defense Authorization Act of 2010 allocated resources for use by the United States Department of Defense (DoD) and mandated that 25% of energy usage by the department be derived from renewable sources by the end of 2025 (U.S. Congress, 2010). One such renewable source is solar energy. This energy source can be captured by PV technology, allowing

absorption of solar radiation to produce electricity via commercially available silicon-based panels. The U.S. Air Force, bearing the majority of the burden imposed by congressional mandate as shown in Figure 1, has made significant investments toward arrays of PV panels at installations such as Nellis Air Force Base (AFB) and Davis-Monthan AFB, utilizing large amounts of real estate readily available at these locations (PEW Project, 2014; U.S. Air Force, 2014).

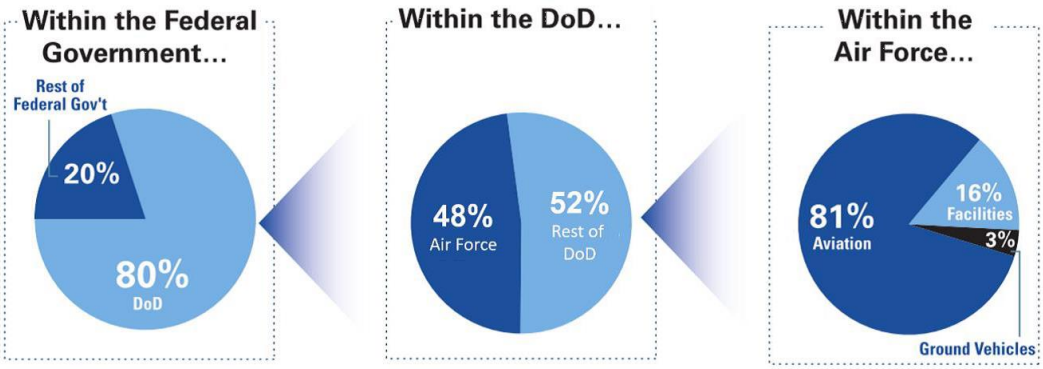

Figure 1. Energy Consumption within the DoD (AFCEC, 2014)

Since military installations may be limited in their available land to an extent that prohibits enterprise-wide adoption of large PV arrays, alternative solutions must be sought. One example is rooftop PV, which requires extensive and costly structural modifications to allow for installation. Because of these challenges, a different method of utilizing PV will be necessary lest the technology be abandoned in favor of renewable energy sources with a higher perceived feasibility.

Great potential exists for the Air Force to continue building energy resilience and complying with congressional mandate. An emerging technology, photovoltaic pavement systems, provided the impetus for this research due to their flat orientation.

Horizontal positioning of PV panels are not normally considered due to decreased efficiency in capturing direct solar radiation. However, there is data that suggests horizontal PV may be more efficient at capturing diffuse solar radiation and may be significantly influenced by temperature and humidity (Brusaw & Brusaw, 2016). In addition, there is a multitude of performance models characterizing power output as a function of temperature and humidity (Sukamongkol et al., 2001; Rosell & Ibanez, 2006; Skoplaki & Palyvos, 2008; Koussa et al., 2012). It is important to note that these models were obtained using tilted panels aimed at maximizing direct radiation exposure. Therefore, insights from current literature apply to applications using tilted panels and not necessarily to those using horizontal panels.

For applications utilizing a horizontal tilt, the goal is assessment of PV performance at different locations around the world comprising a variety of climate types, temperatures, and humidity ranges. There may be many environmental factors to consider in assessing PV performance through multiple successive research efforts. This research narrows its focus to determining performance impacts of temperature and humidity on two types of PV panels: mono-crystalline and poly-crystalline. Currently, 24 and 27 performance models exist for efficiency and power, respectively, with temperature as an independent variable. In addition, the Köppen-Geiger Climate Classification methodology was utilized in a prior study to produce several climate categories in which Air Force installations are located (Nussbaum, 2017). These categories result in a great amount of variance in the effects of ambient temperature and humidity in mono- and poly- crystalline PV panels. The study also identified 25 global

regions in which test systems would need to be placed. Further details on this process, including test site selection, are provided in the following chapter. This effort implements the proposed global test to analyze data gathered from 37 installations in which the Air Force operates. Simultaneous research examines categorical data from this test and performs logistical regression to determine which military installations and their corresponding climate types are ideally suited for horizontal PV panels in any given application. Follow-on studies will build upon the knowledge garnered through this line of research to gain a more complete understanding of the benefits and risks of full investment into this technology.

Problem Statement

As stated in the previous section, there are many performance models characterizing power output as a function of temperature and a considerable number of separate models accounting for humidity. Again, these accounted for non-horizontal PV panels and users of PV technology may be constrained to horizontal positioning of panels. Thus, users would remain unable to predict the amount of electricity produced at any given time due to a lack of data in their respective climates and global positions. A deeper understanding is needed regarding performance at various locations with a broad range of temperature and humidity. This would serve to arm leadership with decision-making power in considering PV-related projects on military installations or within any interested organization.

Research Objectives

To fully analyze and predict power output as a function of temperature and humidity, data must be gathered from as many of the 25 stated global regions as possible to account for any variation due to different climate types. In addition, a dataset spanning a full year is necessary to account for seasonal changes that are likely to have significant impact on panel performance. A larger sample size covering the entire year will hone the resulting regression model's accuracy, with limitations. Data spanning a greater number of years would be required to obtain the most accurate model possible. An analysis of the data allows for comparison with existing performance models to ascertain which most accurately predicts power output over the course of a year. Quality of data that lacks significant gaps or errors is important to establish confidence in the accuracy of new regression models based on ambient temperature and humidity. After constructing a new regression model, a tolerable range of values pertaining to ambient conditions that maximize power output can be discovered.

The aim of this study will be to build upon previous research and implement the proposed study by Nussbaum. The end goal in assessing the feasibility of horizontal PV technology remains. To build toward that end, this study aims to refine the accuracy of existing ambient temperature/humidity dependent performance models that characterize horizontal silicon-based PV panels in a variety of previously identified test regions. Current data gathered by Brusaw and Brusaw only encapsulates latitudes within the U.S., though the Air Force maintains operations at continental U.S. (CONUS) and overseas (OCONUS) installations. Collecting data and identifying performance coefficients at

military installations operating on other continents will provide a more robust performance characterization.

Investigative Questions

Test systems monitoring power output at each test site measured and recorded power readings for an initial period of one year. Time constraints prompted preliminary analysis of data spanning a shorter timeframe, discussed in chapters III and IV. Following data compilation for initial analysis, research utilized multivariate regression techniques to answer the following primary research questions:

1. Which existing model most accurately predicts PV performance with respect to ambient temperature and humidity?
2. How accurate is an empirically established regression model based on ambient temperature, ambient humidity, and global position for mono- and poly-crystalline silicon PV panels?
3. Which ambient conditions are optimal for use of horizontally inclined mono- and poly-crystalline silicon panels?

Methodology Overview

To carry out this study, researchers constructed 40 test systems, each consisting of a 25W mono-crystalline PV panel, a 50W poly-crystalline PV panel, a temperature/humidity probe, a satellite communication module, a central processing unit (CPU), and several other peripheral items. The CPU will control the operation of the other electronic components. Measurements were collected from the PV panels and probe for storage, transmission, and data processing. Three of the test systems remain at AFIT while the other 37 were distributed to test sites around the globe. The test systems

operate by recording power outputs every 15 minutes. Data points include instantaneous values for ambient temperature, humidity, and 64 distinct voltage/current readings for each panel. The technique utilized for this analysis is multivariate linear regression to produce accurate performance models and establish relationships between power output and temperature/humidity for mono-crystalline and poly-crystalline panel types. Other factors such as latitude, longitude, season, month, internal controls temperature and respective power-monitoring node temperatures are included to properly identify the principle components affects performance. To account for possible variation in results from test systems placed on the ground and roof tops, a two-sample t-test is conducted to ascertain significant differences from the two differing surface types.

Assumptions and Limitations

To facilitate this study, assumptions were made with regard to items outside research scope or researcher control. Panels will perform with efficiency consistent with manufacturer specifications. Respective test site climates will remain stable without significant deviations from the norm. Some data gaps are expected to be present as a myriad of issues can arise from the task of keeping 37 global systems operating at all times. Examples of issues include power outages, debris or snow cover, damage from equipment such as lawn-mowers, and bystander interference. It is assumed that site monitors will address issues and notify researchers immediately upon discovery so that exceptions can be noted and accounted for during data analysis.

Limitations pertaining to this study include the sole testing of silicon-based panels amid other PV technologies available on the market. Additionally, funding limitations

reduce margin for error and ability to ship spare parts to test sites should the need arise. For the same reason and in addition to commercial availability, researchers purchased poly-crystalline panels which are two times the size of the mono-crystalline panels. It is possible, though unlikely, that this may affect data quality. Since PV fundamentals dictate power is linearly proportional to panel size, negative effects are expected to be minimal. To control for this, output is reduced to wattage per square foot.

Organization of Thesis

This thesis is organized into a traditional five-chapter format. This chapter will be followed by a review of existing literature summarizing the most current knowledge in the field and providing insight from prominent subject matter experts. Chapter III details the methodology used and will cover test system design, manufacturing, data collection, and analysis methods. Chapter IV presents results garnered from analyzed data. The fifth and final chapter draws conclusions from the resulting analysis and provides readers with possible decision-making information regarding application of PV technology. Lastly, the final chapter discusses further research opportunities

II. LITERATURE REVIEW

This chapter provides readers with a detailed summary of the body of knowledge pertaining to the general use of photovoltaics. National defense requires identification of security vulnerabilities in U.S. power supplies and U.S. Department of Defense (DoD) considerations, necessitating research into alternative fuels and thus prompting this study. The reader can expect a basic overview of photovoltaic principles to understand the basic functionality. Photovoltaic pavement systems, one possible application of horizontal panels and the driver of this study, appear in this chapter to provide readers with information about an effort to implement them in the U.S. Also discussed in this chapter are the global positions and climate types considered for panel positioning during the global test, types of panels included, and horizontal panel orientation. The chapter will conclude with a detailed discussion of currently existing performance models that attempt to characterize performance as functions of temperature, humidity, and other factors.

Energy Security

With regard to national defense, the U.S. Air Force seeks guaranteed energy security by maximizing availability of supplies and the capability of safely providing reliable power for military operations. The U.S. Air Force Energy Strategic Plan enumerates four overarching goals for the service: improve resiliency, reduce demand, assure supply, and foster an energy aware culture (USAF, 2013). These goals are furthered through federal policy and implemented by the service through the Air Force Energy Council. Figure 2 displays this three-tiered governing body, which is responsible

for forming focus groups with the intent to solve problems regarding issues of energy security, aviation operations, and research, development, test, and evaluation (RDT&E).

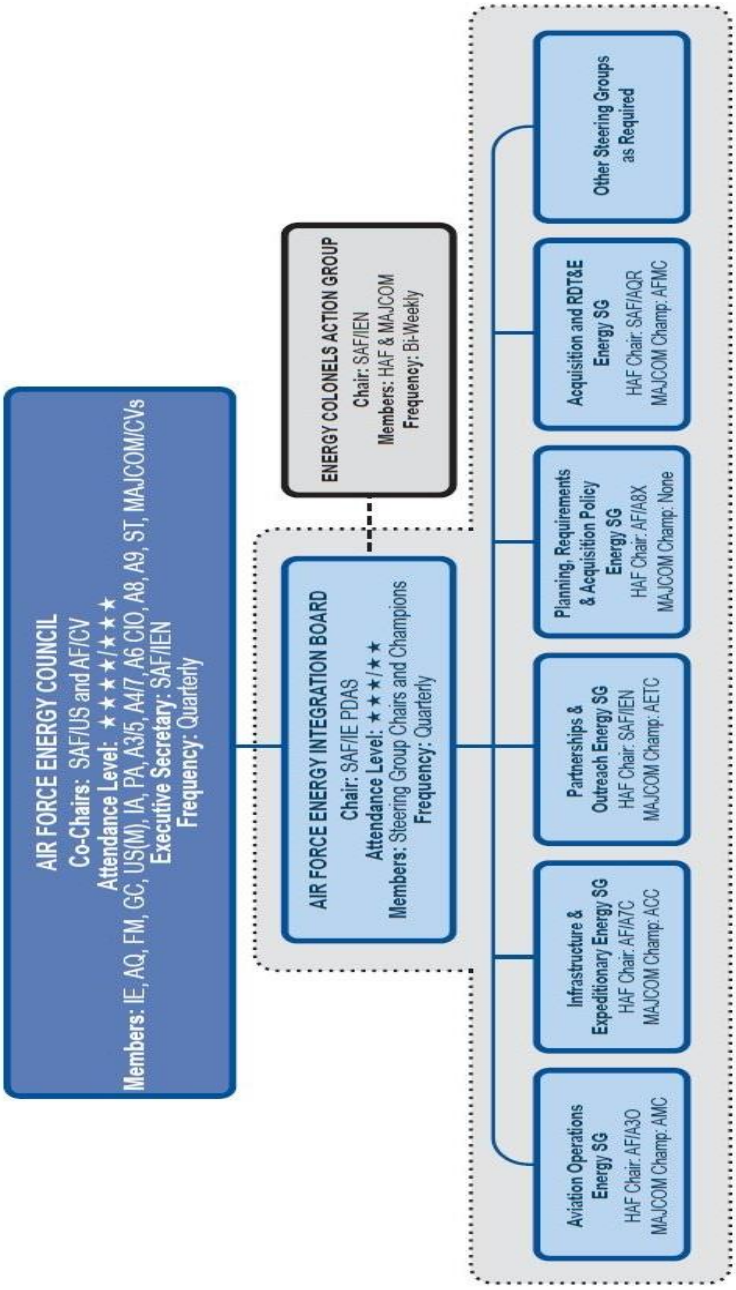

Figure 2. Energy Council Governance Structure (USAF, 2013)

Research into photovoltaics (PV) can have a positive impact to supply assurance while fulfilling public mandates and internal service objectives such as the increased utilization of renewable energy sources. The protection of the U.S. power grid and, by extension, vulnerability of power supplies on military installations has come into focus in recent years. Adequate protection of these resources must be accomplished through physical and cyber security methods.

Vulnerability of U.S. Grid

The federal budget, in alignment with DoD's strategy to defend its networks and U.S. interests from cyber-attacks, will attempt to fulfill the Cyber Mission Force of 133 teams tasked with cyber security by end of Fiscal Year (FY)18. Federal spending is projected to be $6.7 billion in FY17, a 15% increase from FY16, in response to greater cyber security threats (US Department of Defense, 2016).

In March of 2007, an experiment named "Aurora" was conducted to test the resilience of U.S. energy assets by using computers to launch a cyber-attack on a generator at the Department of Energy's Idaho Laboratory. Experimenters were successful in causing the generator to emit smoke, malfunction, and cease operation (Meserve, 2007). This test highlighted the relative ease with which internal or external forces could exploit the U.S. power grid and cause a local or potentially nationwide power failure. A 2017 world-wide cyber-attack using ransomware, software that renders computers inaccessible pending monetary payments to restore system access, renewed concerns regarding U.S. power grid vulnerability. More than 57,000 infections in 99 countries were observed primarily targeting Microsoft Windows operating systems in

Russia, Ukraine, and Taiwan (Volz, 2017). The concern is not just for vulnerability of civilian power, but also for the possible compromise of national defense should military installations be targeted. As ransomware and similar software intended to exploit or destroy become more sophisticated, the DoD is facing a situation prompting exploration of alternative energy options to build a robust power supply network which minimizes the likelihood of and the damage caused in the event cyber-attacks occur.

DoD Considerations

The issue of facility energy consumption has spurred additional legislation to combat the increase in facility energy intensity. The years 2001 through 2006 saw a 40% increase in Air Force energy consumption (AFCEC, 2014). The National Defense Authorization Acts of 2007, 2008, and 2009; the Energy Policy of Act of 2005; and Executive Order 13423 established the federal requirement for 7.5% utilization of renewable energy by 2013 and 25% by 2025 for all federal and DoD facilities, respectively (AFCEC, 2014; Energy Flight Plan, 2017). The U.S. Department of Energy reports that, as of this writing, 8.3% of federal government energy consumption comes from renewable sources (Office of Energy Efficiency & Renewable Energy, 2018). Progress in meeting the DoD's 25% goal remains to be seen. Future considerations regarding vulnerability to attack, climate change, and increased demand will require substantial effort to accommodate. With today's resource constraints, photovoltaics may provide an avenue to directly contribute to the Air Force's pursuit of net zero energy on installations by 2030 and fulfillment of the priority to increase integration of new technologies to reduce costs while leveraging investments (USAF, 2013).

Photovoltaic Basics

PV panels convert sunlight into electricity through the use of thin layers of semi-conducting material. The most common semi-conductor used for this purpose is silicon metal, shown in Figure 3. Silicon-based panels are commercially available in several varieties including monocrystalline, polycrystalline, thin-film, and amorphous. Other semi-conducting material can be used for PV purposes but are not yet widely available or fully tested. Although varying in cost and efficiency, all of these PV types operate under the same basic principles. The most common panel positioning method is adjusting the tilt angle toward the sun to capture direct radiation. Panels are also capable of capturing indirect, or diffuse, radiation caused by airborne water vapor. Further information regarding PV orientation, panel types, and basic principles of PV operation is covered in the remainder of this section.

Figure 3. A chunk of semi-conducting silicon metal (WebElements, 2018)

Operating Principles

The most basic PV unit used to construct larger networks of panels is called a cell, with each cell producing one to two watts of electrical energy (Office of Energy Efficiency & Renewable Energy, 2013). Large arrays of solar cells can be connected in series to produce the desired power output. This makes PV an option for large or small power needs. PV panels, which are most efficient when their flat surface is positioned normal to the sun, produce direct current (DC) which can be used or converted to alternating current (AC) for most power needs such as residential housing. Figure 4 shows a simplified depiction of silicon's arrangement of atoms and electrons, also known as its crystal structure. Each group of dots, represents an atom of silicon (large dot) with four valence electrons in each atom's outer shell, thus resulting in a net neutral charge.

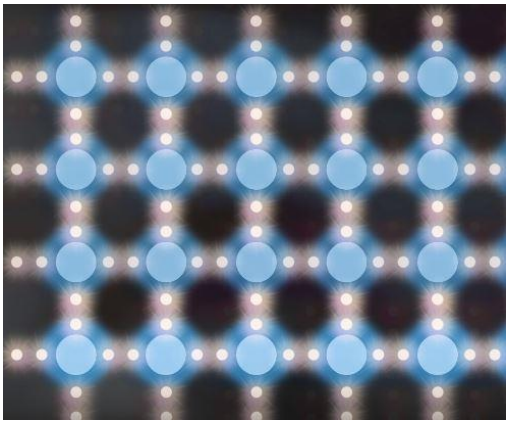

Figure 4. Simplified depiction of crystalline silicon (Laube, 2018)

To enable the silicon to conduct electricity for use in PV applications, impurities are deliberately introduced (a process known as doping) to create an imbalance of electrons resulting in a net-positive or net-negative charge (Laube, 2018). Figure 5

displays the necessary combination of silicon doped with phosphorous (n-type, 5 valance elections) and boron (p-type, 3 valence electrons). This allows photons from incoming sunlight to physically strike excess electrons from the n-type silicon. This leaves a positively charged hole where the electron was previously positioned. Since electrons always tend to flow from the positively charged side to the negative, the freed electron travels away from the n-type silicon to the load, the resulting effect is a 'flow' of holes across the P-N junction from the n-type (extra valance electrons) to the p-type silicon (missing valance electrons) as electrons move to fill in holes closest to the junction. This process repeats to provide a constant flow of charge to the load. The effect is demonstrated in Figures 6 and 7; a more realistic example is depicted using a lightbulb as the load in Figure 8. In Figure 7, note that a hole is still present on the positive side, furthest from the P-N junction. This services as a position to fill for electrons returning from the load

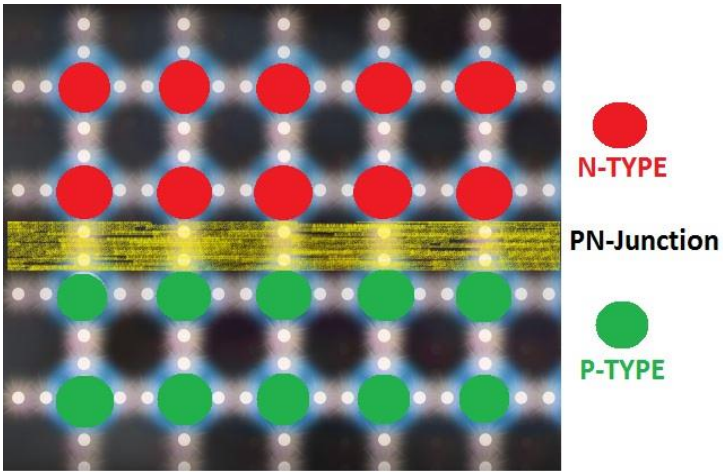

Figure 5. n and p type silicon combined to create a P-N junction

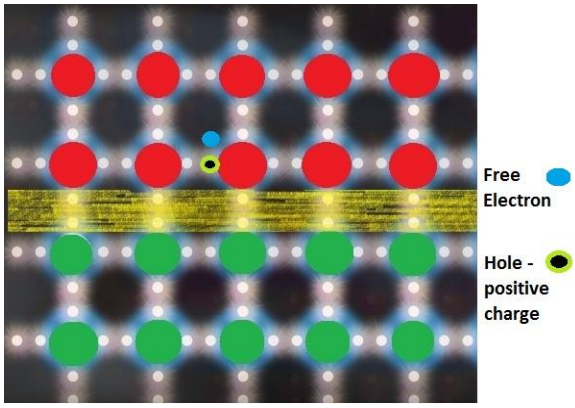

Figure 6. Post-photon strike on PV cell, electron freed

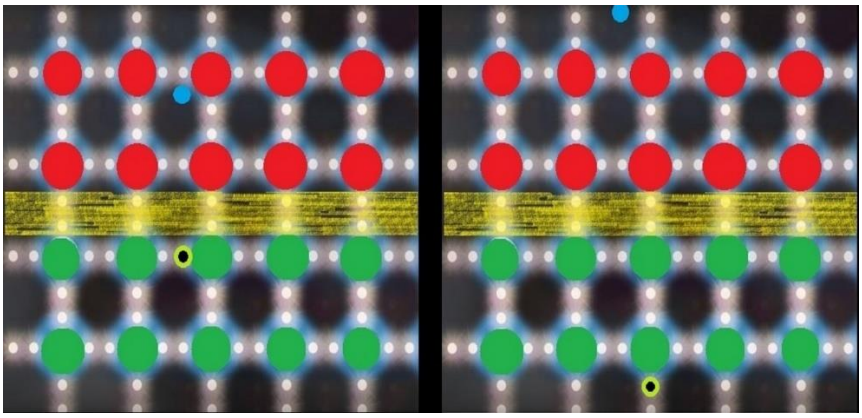

Note: (left to right) holes filled by other electrons. Notice the hole appears to travel away from P-N junction as previous positions are occupied

Figure 7. freed electron flow

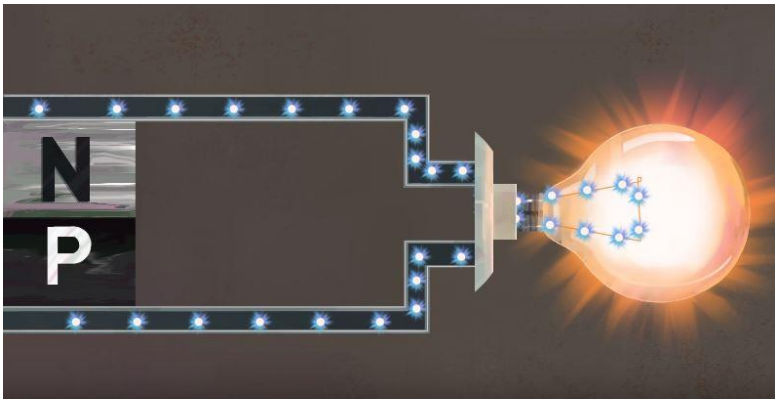

Figure 8. Electron flow, n-type SI, through load, back to p-type SI (TechyChaps, 2017)

Electrons flow through a circuit within a closed loop; therefore, as photons continually bombard the silicon's extra valance electrons free, they will flow through the load and back to the positive side to fill in the rogue hole. This process is more easily seen in Figure 8. The same principles are exploited regardless of specific PV application. Several types of panels are available today that make use of these principles and are discussed in the following section.

Panel Type

A sample of different PV types are displayed in Figure 9. Note that the amorphous cell on the displayed calculator is visible on its upper right corner. These panels differ in appearance, efficiency, and other attributes. Monocrystalline cells have a more complicated, higher cost manufacturing process and result in about 15% efficiency (National Energy Foundation, 2017). In other words, monocrystalline panels can convert approximately 15% of the sunlight striking it to electricity. Polycrystalline, or multicrystalline, cells are slightly cheaper than monocrystalline ones due to a simplified manufacturing process and a lower efficiency of approximately 12% (National Energy Foundation, 2017). Approximately 85% of the U.S. PV market is comprised of the crystalline variety (Maehlum, Which Solar Panel Type is Best? Mono- vs. Polycrystalline vs. Thin Film, 2017). Their availability combined with higher demonstrated efficiency makes them the mostly likely candidate for any given PV application (Nagangast, Hendrickson, & Matthew, 2013). Thin-film silicon is another option which comprises 11% of market penetration and can achieve up to 20.4% efficiency depending on the type. The most common type is amorphous silicon (a-Si), which has an efficiency of

13.4% and higher manufacturing cost, thus making it a sensible option for small, low-power applications such as calculators (Maehlum, 2015). Other variations of thin-film technology are cadmium telluride (CdTe) and copper indium gallium selenide (CIS/CIGS), which are currently emerging technologies with higher efficiencies and expected market share growth (Maehlum, 2015; Mekhile, Saidur, & Kamalisarvestani, 2012). Studies involving non-crystalline panel technologies have yielded significant discrepancies between resulting performance models (Cameron, Boyson, & Riley, 2008) Due to the significantly lower market share of non-crystalline technologies and limited research budgets, these panel types are not used in this research, which instead focuses on commercially abundant crystalline panels.

Note: Monocrystalline (upper left), polycrystalline (upper right), thin film (lower left), and amorphous (lower right) PV cells

Figure 9. Various PV types (Maehlum, 2017)

Sandia National Laboratories has conducted studies to validate existing PV performance models and produce an annual model accounting for the non-proportional output of PV panels comprised of different technologies. Primary emphasis was placed on models that are readily available through a number of U.S. Department of Energy

(DoE)-sponsored calculation tools such as Solar Advisor Model (SAM), PVWATTS, PVFORM, and PVMod. One-year studies were conducted on three different test systems installed without shading and at latitude tilt; the first two systems, utilizing 210 and 220 watt panels, respectively, were comprised of five in-series crystalline silicon panels connected to a 2 kW inverter. The third system contained two strings of seven silicon panels connected to a 2.5 kW inverter. These systems were used to validate radiation, panel output, and inverter output performance submodels in the calculation tools mentioned previously. The results were conclusive for crystalline technologies, showing modeled and experimental results were in agreement within a margin of 3%. Non-crystalline technologies, such as thin-film, showed significant disagreement between models (Cameron, Boyson, & Riley, 2008). As previously mentioned in Chapter I, the effect of tilt angles was not studied. This necessitates further study to validate or produce new models to predict PV performance with a horizontal tilt. For these reasons, current research focuses on evaluating the crystalline variety placed flat on a surface.

Panel Orientation

The most efficient currently known method of capturing sunlight is exposure to direct rays by positioning panels normal to incoming photons. Global latitude is the primary piece of positional data that dictates optimal tilt angle of PV panels for maximum electricity-producing efficiency (Landau, 2015). However, emerging data suggests that horizontal panels (zero degree tilt angle) may perform more efficiently than conventional systems in overcast conditions because of their greater exposure to diffuse irradiance. This insight has spurred current research to explore the potential of utilizing horizontal

PV technology for new applications within regions where solar irradiance is not optimal for traditional PV installation (Brusaw & Brusaw, 2016). In addition, a study was conducted to explore the performance impact of different sun tracking systems (Koussa, Haddadi, Saheb, Malek, & Hadji, 2012). Researchers tested two fixed panel, two single rotating axes, and one two-axis system and calculated the amount of direct, diffuse, and reflected solar irradiance encountered by each. The five configurations were used in the hot and dry Algerian desert to determine and compare power outputs from each of the five systems. As expected, the ability of panels to capture direct beam irradiance was affected by different trackers. Interestingly, it was also found that cloudy days yielded the same power output regardless of the presence of a sun-tracking system. Further, horizontal PV panels performed best during completely cloudy days when compared to inclined, one-axis and two-axis sun tracking systems. Further evidence of increased horizontal panel output on cloudy days has been observed. The observations were made by a U.S.-based company specializing in design and testing of a proprietary PV product utilizing horizontal PV cells. These cells are embedded between tempered glass to produce a potential alternative to traditional pavement. This product provided the impetus for this research and is discussed in the following section.

Photovoltaic Pavement Systems

Military installations are far from suffering a shortage of sidewalks, streets, parking lots, and other pavement. The emergence of PV pavement systems may have the potential to out-produce conventional systems through sheer amounts of area available for PV coverage. One U.S.-based company, Solar Roadways, Incorporated (SRI) is

currently conducting test and evaluation of their product which consists of assembled hexagonal units containing 48W silicon-based solar cells embedded between tempered glass and polymer insulation. A sample of the product is displayed in Figure 10. The product also features other capabilities such as self-heating, light-emitting diodes (LED) to replace road paint, and integrated drainage (Brusaw & Brusaw, 2016). The PV units are intended to be placed on a flat surface which raises questions as to their efficiency and ability to effectively generate electricity.

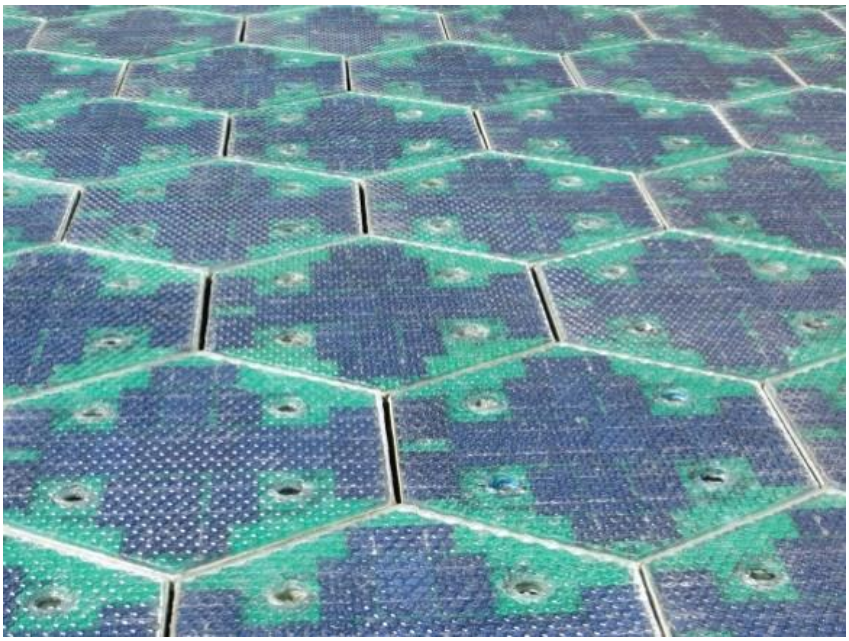

Figure 10. SRI's product - photovoltaic pavement system (Brusaw & Brusaw, 2016)

Performance testing is being conducted using store-bought silicon panels. Each of three test sites, the latest of which is located at the Missouri Department of Transportation as of March 2016 and shown in Figure 11, is equipped with one flat panel and one angled panel to compare variation in results. The first test site was installed in April 2015 at the Biosphere 2 in Oracle, Arizona, while the second test site was installed

in August 2015 at SRI's facility in Sagle, Idaho. The first public test of this product has been taking place since late 2016 in Sandpoint, Idaho, shown in Figure 12. Preliminary analysis of PV performance data collected at different latitudes suggest that flat panels generate more electricity than tilted panels during overcast conditions (Brusaw & Brusaw, 2016). Additionally, total monthly energy produced is comparable between the tilted and horizontal panels. Table 1 displays the most recent results from the Arizona site in which outputs from each panels appear almost the same. Similar results are provided for the other test sites.

Figure 11. Test site at Missouri DOT (Brusaw & Brusaw, 2016)

Figure 12. First public test in Sandpoint, Idaho (Fingas, 2016)

Table 1. One year of test data in Oracle, AZ

Location	Oracle, AZ	
Latitude	32º34′47.38″ N	
Micro-inverter #	2452 (flat panel)	2369 (angled panel)
2015 May	44.1 kWh	44.1 kWh
2015 Jun	41.2 kWh	39.9 kWh
2015 Jul	35.3 kWh	34.4 kWh
2015 Aug	36.6 kWh	37.8 kWh
2015 Sep	30.2 kWh	34.3 kWh
2015 Oct	27.1 kWh	33.8 kWh
2015 Nov	24.4 kWh	35.5 kWh
2015 Dec	19.7 kWh	29.7 kWh
2016 Jan	22.1 kWh	32.3 kWh
2016 Feb	28.7 kWh	39.3 kWh
2016 Mar	35.8 kWh	43.8 kWh
2016 Apr	40.0 kWh	42.9 kWh
2016 May	45.8 kWh	47.1 kWh

It is hypothesized that the similar results are caused by the scattering of photons through airborne water vapor, thus allowing for easier harvesting of diffuse radiation by flat panels than angled panels. Successfully replicating this data for a variety of latitudes and climate conditions may prove the PV pavement application feasible for installations without sufficient sunlight to justify investing in a PV array which is intended to capture direct beam sunlight. Prior research has been conducted by Nussbaum (2017) to determine the applicability of PV panels for energy production on DoD installations. His study provided the foundation for further research into the potential application of horizontal PV on DoD installations through the methodical selection of test locations for horizontal PV systems.

Global Position and Climate Types

The Köppen-Geiger Climate Classification system is used to divide the globe into five main climate zones as shown in Figure 13. The system further divides each zone into a multitude of varying climate types. Previous research utilized this system to ascertain variance in environmental factors affecting PV performance. These factors are largely dependent on latitude, temperature, humidity, and changes in air mass (Nussbaum, 2017). Statistical analysis of 1,763 Air Force installations placed them into bins representing latitude and longitude. From this analysis, 25 regions were identified in which PV system performance could be measured to represent latitudinal and longitudinal effects of temperature and humidity. These regions are listed in Table 2. Subsequent Pareto analysis, a statistical technique used to select principle components that produce the greatest overall effects on performance, established the regions in which

test systems should be placed to gather performance data representing the entire set of installations. As of this writing, concurrent research at AFIT uses this classification system to perform logistical regression based on the interactions between global position and climate types. Additionally, the Air Force operates installations in tropical, dry, temperate, and boreal climate types. Consequentially, the polar climate type will not be included in this round of research.

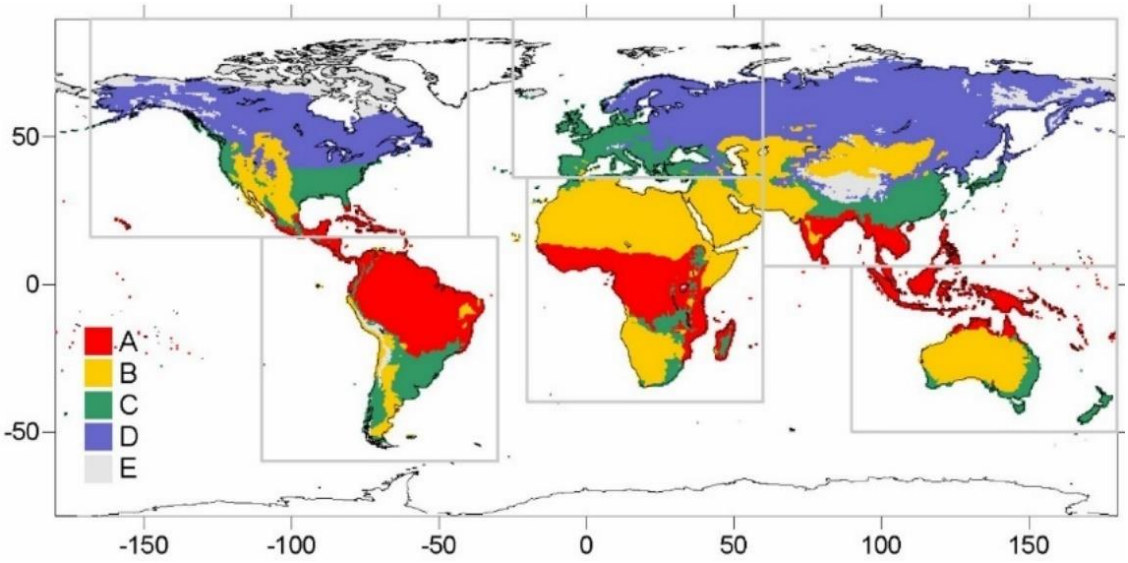

Note: A-Tropical, B-Dry, C-Temperate, D-Boreal, E-Polar

Figure 13. Köppen climate types (Beck, Grieser, & Rubel, 2005)

Table 2. Climate types and locations analyzed (Nussbaum, 2017)

Region	Site	Lat	Long	MAIN/PRECIP	PRECIP/TEMP
A	Site 1:	20.75	-156.25	/Fully Humid	Fully Humid/
C	Site 1:	12.25	-69.25	Arid/Steppe	Steppe/Hot Arid
D	Site 1:	11.75	43.25	Warm Temperate/Summer Dry	Summer Dry/Warm Summer
E	Site 1:	-22.25	114.25	Arid/Desert	Desert/Hot Arid
G	Site 1:	32.75	-106.25	Arid/Steppe	Steppe/Cold Arid
G	Site 2:	29.25	-100.25	Arid/Steppe	Steppe/Hot Arid
G	Site 3:	34.25	-103.25	Arid/Steppe	Steppe/Cold Arid
G	Site 4:	33.75	-117.25	Warm Temperate/Summer Dry	Summer Dry/Hot Summer
H	Site 1:	31.25	-92.75	Warm Temperate/Fully Humid	Fully Humid/Hot Summer
H	Site 2:	25.75	-80.25	/Fully Humid	Fully Humid/
I	Site 1:	33.25	19.75	Arid/Desert	Desert/Hot Arid
J	Site 1:	33.75	130.25	Warm Temperate/Fully Humid	Fully Humid/Hot Summer
L	Site 1:	40.75	-113.25	Arid/Steppe	Steppe/Cold Arid
L	Site 2:	41.25	-95.75	Snow/Fully Humid	Fully Humid/Hot Summer
L	Site 3:	38.25	-121.75	Warm Temperate/Summer Dry	Summer Dry/Hot Summer
L	Site 4:	38.75	-104.75	Arid/Steppe	Steppe/Cold Arid
L	Site 5:	38.75	-104.75	Arid/Steppe	Steppe/Cold Arid
L	Site 6:	41.25	-111.75	Snow/Fully Humid	Fully Humid/Warm Summer
M	Site 1:	40.75	-86.25	Snow/Fully Humid	Fully Humid/Hot Summer
M	Site 2:	37.25	-76.25	Warm Temperate/Fully Humid	Fully Humid/Hot Summer
M	Site 3:	40.25	-74.25	Warm Temperate/Fully Humid	Fully Humid/Hot Summer
M	Site 4:	44.75	-93.25	Snow/Fully Humid	Fully Humid/Hot Summer
N	Site 1:	38.75	-27.25	Warm Temperate/Summer Dry	Summer Dry/Warm Summer
O	Site 1:	39.75	125.25	Snow/Winter Dry	Winter Dry/Hot Summer
O	Site 3:	37.25	128.75	Snow/Winter Dry	Winter Dry/Hot Summer
P	Site 1:	55.25	-162.75	Warm Temperate/Fully Humid	Fully Humid/Cool Summer
Q	Site 1:	47.75	-101.25	Snow/Fully Humid	Fully Humid/Warm Summer
Q	Site 2:	47.25	-122.75	Warm Temperate/Summer Dry	Summer Dry/Warm Summer
Q	Site 4:	48.25	-101.25	Snow/Fully Humid	Fully Humid/Warm Summer
Q	Site 5:	47.75	-111.25	Arid/Steppe	Steppe/Cold Arid
R	Site 1:	46.75	-67.75	Snow/Fully Humid	Fully Humid/Warm Summer
S	Site 1:	50.25	6.75	Warm Temperate/Fully Humid	Fully Humid/Warm Summer
T	Site 1:	52.75	174.25	Snow/Fully Humid	Fully Humid/Cool Summer
U	Site 1:	64.25	-149.25	Snow/Fully Humid	Fully Humid/Cool Summer
U	Site 2:	65.75	-167.75	Polar/	/Polar Tundra
W	Site 1:	76.75	-68.75	Polar/	/Polar Tundra
X	Site 1:	58.75	5.75	Warm Temperate/Fully Humid	Fully Humid/Warm Summer

Temperature and Humidity Performance Models

Many competing equations exist describing efficiency and power output as functions of temperature. Functions that utilize ambient temperature yield more variance. As shown in Tables 3 and 4, respectively, there are currently 24 functions describing efficiency and 27 describing power (Skoplaki & Palyvos, 2008; Rosell & Ibanez, 2006). Global research is first intended to center on the effects of temperature and humidity on mono- and poly-crystalline PV panels to refine existing performance models using empirical data. Humidity has been shown to have a substantial direct and indirect influence on PV performance. Directly, visible and microscopic water droplets divert incoming photons through refraction, diffraction, and reflection. Indirectly, dust build-up, in significant amounts, creates a barrier to photons striking the doped silicon within the PV panels and thus reducing power output. It is estimated that between 1 and 65.8 percent of potential PV output is lost due to these effects, directly depending on the percentage of solar rays blocked (Mekhile, Saidur, & Kamalisarvestani, 2012).

Existing models for predicting the performance of PV panels have been produced by Sandia National Laboratories and are supported by the U.S. Department of Energy (DoE) (Cameron, Boyson, & Riley, 2008). Further validation and refinement of these models has been conducted to improve the accuracy of predictions against empirical results. Typical tests are concerned with panels tilted at latitude and toward the sun for maximum energy output.

Additional modeling efforts in sunny and cloudy conditions have included the panel fill factor (FF) in addition to short-circuit current, open-circuit voltage, and maximum power output as variables dependent on solar intensity and model temperature.

The findings confirm weather's strong influence on irradiance captured by PV (Wei, Yang, & Fang, 2007). Most of the research requires humidity as an independent variable in their respective performance models while all require temperature. Refining these functions for PV system performance will allow users to determine the optimum size of the system for specific load requirements under local meteorological conditions.

Table 3. Competing Temperature/Efficiency Equations (Skoplaki & Palyvos, 2008)

Correlation	Comments	Ref.
$\eta_T = \eta_{T_{ref}}\left[1-\beta_{ref}\left(T-T_{ref}\right)\right]$	$T_{ref}=25$ °C, $\eta_{T_{ref}}=0.15$, $\beta_{ref}=0.0041$ °C^{-1}, c-Si, T in °C	Evans and Florschuetz (1977)
$\eta_{PV}=\eta_{ref}-\mu(T_c-T_{ref})$	μ = overall cell temperature coefficient	Bazilian and Prasad (2002)
$\eta=\eta_a-c(\overline{T}-T_a)$	$\overline{T}$ = mean solar cell temp, η_a = efficiency at T_a, c = temperature coefficient	Bergene and Løvvik (1995)
$\eta=\eta_{25}+b(T_c-25)$	$b=b(G_T)$, T in °C	Durisch et al. (1996)
$\eta(G_T,T_c)=\eta(G_T,25\,^\circ\text{C})[1+c_3(T_c-25)]$	$c_3=-0.5$ (% loss per °C) for c-Si, -0.02, …, -0.41 for thin film cells	Mohring et al. (2004)
$\eta_T=\eta_0-K(T^{1/4}-T_0^{1/4})$	$T_0=273$ K, $K=22.4$	Ravindra and Srivastava (1979/80)
$\eta_a=\eta_n\times k_\gamma\times k_\theta\times k_\alpha\times k_\lambda$ with $k_\gamma=1-\gamma(T_c-25)/100$	k_γ = power temperature coefficient, k_j, $j=\theta$, α, λ optical, absorption, spectrum correction factors	Aste et al. (2008)
$\eta=\eta_{T_{ref}}\left[1-\beta_{ref}\left(T_a-T_{ref}\right)-\frac{\beta_{ref}\tau\alpha G_T}{U_L}\right]$	5% low predictions, $\beta_{ref}\sim0.004$ °C^{-1}, $\eta_{T_{ref}}=0.15$, $T_{ref}=0$ °C	Siegel et al. (1981)
$\bar{\eta}=\eta_{T_{ref}}\left[1-\beta_{ref}\left(\overline{T}_a-T_{ref}\right)-\frac{\beta_{ref}\left(\frac{\tau\alpha}{U_L}\right)\overline{H}_T}{nU_L}\right]$	$\bar{\eta}$ = monthly average efficiency, V = dimensionless, $\beta_{ref}\sim0.004$ °C^{-1}	Siegel et al. (1981)
$\eta_i=\eta_{T_{ref}}\left[1-\beta_{ref}\left(T_{c,i}-T_{ref}\right)+\gamma\log_{10}I_i\right]$	η_i = hourly efficiency, I_i = incident hourly insol, $\beta_{ref}\sim0.0045$ °C^{-1}, $\gamma\sim0.12$	Evans (1981) and Cristofari et al. (2006)
$\eta=\eta_{T_{ref}}\left[1-\beta_{ref}(T_c-T_{ref})+\gamma\log_{10}G_T\right]$	η = instantaneous efficiency, $\beta_{ref}=0.0044$ °C^{-1} $\eta_{T\,ref}=0.125$, $T_{ref}=25$ °C	Notton et al. (2005)
$\bar{\eta}=\eta_{T_{ref}}\left\{1-\beta_{ref}\left[(T_c-T_a)-(T_a-\overline{T}_a)-(\overline{T}_a-T_{ref})\right]+\gamma\log_{10}I\right\}$	$\bar{\eta}$ = monthly average efficiency, $\beta_{ref}\sim0.0045$ °C^{-1}, $\gamma\sim0.12$	Evans (1981)
$\eta=\eta_{ref}\left[1-a_1(T_c-T_{ref})+a_2\ln(G_T/1000)\right]$	For Si $a_1=0.005$, $a_2=0.052$, omitting the ln term slightly overestimates η	Anis et al. (1983)
$\eta(XG_T,T)=\eta(G_T,T_{ref})\left[1-\beta_{ref}(T-T_0)\right]\left(1+\frac{k_BT}{q}\frac{\ln X}{V_{oc}(G_T,T_0)}\right)$	X = concentration factor, for $X=1$ it reduces to Eq. (2)	Lasnier and Ang (1990)
$\eta=\eta_{ref}\left\{1-\beta\left[T_a-T_{ref}+(T_{NOCT}-T_a)\frac{G_T}{G_{NOCT}}\right]\right\}$	The T_c expression from Kou et al. (1998) is introduced into the η expression in Evans and Florschuetz (1977)	–
$\eta=\eta_{ref}\left\{1-\beta\left[T_a-T_{ref}+\left(\frac{9.5}{5.7+3.8V_w}\right)(T_{NOCT}-T_a)\frac{G_T}{G_{NOCT}}\right]\right\}$	The T_c expression from Duffie and Beckman (2006) is introduced into the η expression in Evans and Florschuetz (1977)	–
$\eta=\eta_{ref}\left[1-0.9\beta\frac{G_T}{G_{T,NOCT}}\left(T_{c,NOCT}-T_{a,NOCT}\right)-\beta\left(T_a-T_{ref}\right)\right]$	Assumes $\eta\approx0.9(\tau\alpha)$	Hove (2000)
$\eta_{nom}=-0.05T_{surface}+13.75$	$T_{surface}=1.06T_{back}+22.6$	Yamaguchi et al. (2003)
$\eta_{meas}=-0.053T_{back}+12.62$	Nominal vs measured values	
$\eta=a_0+a_1\frac{T_c(x,t)-T_\infty}{T_\infty}+a_2\frac{G_T-G_{ref}}{G_{ref}}$	A_k, $k=0$, 1 and 2 are empirical constants, T_∞ is the indoor ambient temperature	Zhu et al. (2004)
$\eta_{MPP}(G_T,T)=\eta_{MPP}(G_T,25\,^\circ\text{C})(1+\alpha(T-25))eta_{MPP}(G_T,25\,^\circ\text{C})$ $=a_1+a_2G_T+a_3\ln(G_T)$	a_1–a_3 device specific parameters, MPP tracking system	Beyer et al. (2004)
$\eta=\eta_{NOCT}[1-MPTC(T_{NOCT}-T_c)]$	$MPTC$ = maximum power temperature coefficient[a]	Perlman et al. (2005)
$\eta=a+b\frac{T_{in}-T_a}{G_T}$	PV/T collector. PV cover: 100% → $a=0.123$, $b=-0.464$; 50% → $a=0.121$, $b=-0.450$	Chow et al. (2006)
$\eta=0.94-0.0043\left[\overline{T}_a+\frac{\overline{G}_T}{(22.4+8.7\overline{V}_w)}-25\right]\pm2.6\%$	Overbars denote daily averages. $\overline{G}_T$ = Wh/m^2 received/length of day (h) $\overline{V}_w$ in m/s	CLEFS CEA (2004)

Notes:

- In Bücher (1997): PRT factor temperature effect on PV performance.
- In Oshiro et al. (1997): KPT cell temperature factor.
- In Jardim et al. (2008): NOCT-corrected efficiency.

[a] With MPTC = −0.5% loss per °C, the efficiency is $\eta=11.523-0.0512T_c$.

Table 4. Competing Temperature/Power Equations (Skoplaki & Palyvos, 2008)

PV array power as a function of temperature $P = \eta_c A G_T$.

Correlation	Comments	References
$P = \eta_{T_{ref}} A G_T (\tau\alpha)[1 - \beta_{ref}(T_P - T_{ref})]$	T_P = plate temperature, $\eta_{T_{ref}} = 0.118$ at 45 °C – air coll, $\eta_{T_{ref}} = 0.108$ at 28 °C – water coll	Hendrie (1979)
$P_{T_c} = \eta_{ref} A G_T K_f [1 + \alpha(T_c - 25)]$	$T_{ref} = 25$ °C, $\eta_{T_{ref}} = 0.13$, $\alpha = -0.004$ °C^{-1}, K_f factor for rest, frame installation, T_c in °C	Nishioka et al. (2003)
$P = \eta_e A G_T \tau_g p[1 - \beta_{ref}(T_c - 25)]$	p = packing factor, T_c in °C, τ_g = glazing transmissivity	Chow et al. (2006)
$P = \eta_{T_{ref}} A G_T [1 - 0.0045(T_c - 298.15)]$	$\eta_{T_{ref}} = 0.14$, T_c in K	Jie et al. (2007a)
$P = \eta_{T_{ref}} A G_T \tau_{pv} [1 - 0.0045(T_c - 25)]$	$\eta_{T_{ref}} = 0.14$, T_c in °C, τ_{pv} = pv cell glazing transmittance	Jie et al. (2007b)
$P = \eta_{T_{ref}} A G_T [1 - \beta_{ref}(T_c - T_{ref}) + \gamma \log_{10} G_T]$	$\beta_{ref} = 0.0044$ °C^{-1} for pc-Si, γ is usually taken as 0	Cristofari et al. (2006)
$P_T = P_{ref}[1 - \beta_{ref}(T - T_{ref})]$	$\beta_{ref} = 0.004$–0.006 °C^{-1}, T in °C, T_{ref} = reference temperature	Buresch (1983)
Same as above	$\beta_{ref} = 0.004$	Twidell and Weir (1986)
$P(T) = P(25)[1 - \gamma(T - 25)]$	$\gamma = 0.0053$ °C^{-1} for c-Si range: 0.004–0.006 °C^{-1}	Parretta et al. (1998)
$P_T = P_{25}[1 - 0.0026(T - 25)]$	a-Si, T in °C, power degrades to $0.82 P_{init}$	Yamawaki et al. (2001)
$P_T = P_{25} + \frac{dP}{dT}(T - 25)$	$\frac{dP}{dT} = -0.00407, -0.00535$, Si space cells, T in °C	Osterwald (1986)
$P(T) \approx G_T[\eta_0 - c(T - T_a)]$	η_0 = efficiency at T_a, c = temperature dependence factor	Bergene and Løvvik (1995)
$P_{max} = P_{max,ref}[1 - Df(T_c - 25)]$	Df = "deficiency factor" = 0.005 °C^{-1}	Al-Sabounchi (1998)
$P_{\max} = P_{\max,ref} \frac{G_T}{G_{T,ref}}[1 + \gamma(T_c - T_{ref})]$	γ = temperature factor for power, $\gamma = -0.0035$ (range – 0.005 °C^{-1} to −0.003 °C^{-1}). T_c in °C	Menicucci and Fernandez (1988)
$P_{max} = P_{max,ref} \frac{G_T}{G_{T,ref}}[1 + \gamma(T_c - 25)]$	$\gamma = -0.0035$ (range – 0.005 °C^{-1} to −0.003 °C^{-1}) T_c in °C	Fuentes et al. (2007)
$P_{\max} = P_{\max,ref} \frac{G_T}{1000}[1 + \gamma(T_c - T_{ref})]$	γ = temperature factor for power, $T_{ref} = 25$ °C, used in PVFORM	Marion (2002)
$P_{mp,T_r} = I_{mp,T}[1 - \alpha(T - T_r)]\left[V_{mp,T} - \beta V_{mp}^{STC}(T - T_r)\right]$	*STC* refers to ASTM standard conditions (1000 W/m^2, AMI = 1.5, $T_r = 25$ °C)	King et al. (1997)
$P_{max} = P_{max,ref} \frac{G_T}{G_{T_{ref}}}[1 + \alpha(T - T_{ref})][1 + \beta_{ref}(T - T_{ref})]\left[1 + \delta(T)\ln\left(\frac{G_T}{G_{T_{ref}}}\right)\right]$	Adapted from the MER model[a]. Coefficient δ evaluated at actual conditions	Kroposki et al. (2000)
$P = P_0[1 + (\alpha - \beta_{ref})\Delta T]$	α: 0.0005 °C^{-1}, β: 0.005 °C^{-1}	Patel. (1999)
$P = (\alpha T_c + \beta) G_T$	α = temperature coefficient, β = calibration constant	Yang et al. (2000)
$P = -4.0 + 0.053 G_T + 0.13 T_c - 0.00026 G_T T_c$	MPPTracked 100 kWp system	Risser and Fuentes (1983)
$P = -0.4905 + 0.05089 G_T + 0.00753 T_c - 0.000289 G_T T_a$	MPPTracked 100 kWp system	Risser and Fuentes (1983)
$P_T = -8.6415 + 0.076128 G_T + 1.02318 \times G_T^2 + 0.20178 T - 4.9886 \times 10^{-3} T^2$	T is the panel temperature (K), too many significant figures!!!	Jie et al. (2002)
$P = G_T(b_1 + b_2 G_T + b_3 T_a + b_4 V_f)$	EPTC model, b_j regression coefficients, V_w^f wind speed 10 m above ground	Farmer (1992)
$P = c_1 + (c_2 + c_3 T_a) G_T + (c_4 + c_5 V_w) G_T^2$	c_j regression coefficients based on STC module tests[b]	Taylor (1986)
$P_{mp} = D_1 G_T + D_2 T_c + D_3[\ln(G_T)]^m + D_4 T_c[\ln(G_T)]^m$	D_j (j = 1–4), m parameters[c]	Rosell and Ibáñez (2006)
$P = V_c I_c\left[1 - \frac{G_T - 500}{2.0 \times 10^{-4}} + \frac{C_{T_c}}{4 \times 10^4}(50 - T_c)^2\right]$	I_c = output current (A), V_c = output voltage (V), T_c in K, $C_{T_c} = 1$ if $T_c \leqslant 50$ °C or =3 if $T_c \geqslant 50$ °C	Furushima et al. (2006)
$P = A(0.128 G_T - 0.239 \times 10^{-3} T_a)$	p-Si, hybrid PV-fuel cells system G_T in kW/m^2, P in kW, T_a in °C	Zervas et al. (2007)
$P = P_{ref} G_T K_{pt} K_w K_e K_c$ with $K_{pt} = 1 + \alpha(T_c - 25)$	K_w, K_e, K_c loss coefficients due to mounting, dirt etc., AC conversion. Semitransparent PV	Wong et al. (2005)

Notes:

- Ref. Bücher et al. (1998): reports power temperature coefficients for various module types in the range [−0.0022/K to 0.0071/K], values around −0.002 referring to a-Si.
- Refs. Radziemska (2003) and Radziemska and Klugmann (2006): report power temperature coefficients −0.0065/K for c-Si.
- Ref. Fathi and Salem (2007): reports a dimensional expression for "power" – actually specific energy!
- Energy production correlation E_{out} {W hr} $= (\varepsilon_0 + \varepsilon_1 T_c) E$ {kW hr/m^2}, with $36.41 \leqslant \varepsilon_0 \leqslant 44.14$ and $-0.20 \leqslant \varepsilon_1 \leqslant -0.16$ is given in del Cueto (2001).
- Daily energy production (W h/day) is given by $E = A_1 H + A_2 H (T_{a,max})^{-2} + A_3 T_{a,max}$, with $T_{a,max}$ the maximum ambient temperature (°C), H the daily total insolation (W h/m^2/day) and A_j regression coefficients, according to the EMAT model (Meyer and van Dyk, 2000).
- Ref. Zhou et al. (2007) presents an expression for P_{max} based on BIPV data, which, for two states 0 and 1, is proportional to $(T_0/T_1)^\gamma$ with $\gamma = \frac{\ln(V_{oc_0}/V_{oc_1})}{\ln(T_1/T_0)}$.
- There are few equations with no explicit temperature dependence. Among them, the single regression yearly average form $P_{yr} = 0.1103 G_{T,yr}$ (Liu et al, 2004) and the nonlinear expression $P = c_1 G_T + c_2 G_T^2 + c_3 G_T \ln G_T$, with c_j regression coefficients, known as the ENRA model (Gianolli Rossi and Krebs, 1988), which over-predicts the PV performance.

[a] The V_{oc} and I_{sc} expressions have been combined as in Eq. (1).

[b] The regression equation shown combines the original equation for P and the analogous expression for T_c.

[c] For pc-Si, $D_1 = 0.000554$, $D_2 = -7.275 \times 10^{-5}$, $D_3 = 2.242 \times 10^{-5}$, $D_4 = -4.763 \times 10^{-8}$, $m = 7.0306$. Analogous sets are given for c-Si, a-Si, and thin film modules.

The cited study which determined optimal sun-tracking configuration used only one proposed model predicting PV behavior and is described by the equation,

$$I = I_L - I_0\left[\exp\left(\frac{q}{\gamma_p k T_c}\right)(V + IR_s) - 1\right]$$

where q is the charge on an electron (1.602×10^{-19} C), k is Boltzmann's constant (1.381×10^{-23} J/°K), T_c is the solar cell temperature, I is the operating current (A), V is the operating voltage (V), I_L is the photocurrent, and I_0 is the diode reverse saturation current. The γ_p and R_s factors are the empirical photovoltaic curve fitting parameter and model series resistance, respectively (Koussa, Haddadi, Saheb, Malek, & Hadji, 2012). Note that humidity does not appear in this model, although previously cited data suggests humidity significantly affects the PV's ability to capture diffuse solar radiation. To properly utilize horizontal PV systems, especially in regions with little sunlight and persistently overcast conditions, capturing the maximum amount of diffuse radiation is paramount. Therefore, a performance model that can accurately predict power output as functions of temperature and humidity is necessary to ascertain the feasibility of using horizontal orientation at any global location.

III. METHODOLOGY

Little research has been done with respect to horizontal photovoltaic (PV) panels and current research is inspired by existing methods of data collection and analysis covered in Chapter II. Since this line of research builds upon a prior feasibility study, the methods for data collection and selection of test sites have already been established. Test system design and prototyping was conducted by a team of AFIT graduate students while this phase of the research carried out manufacturing and distribution of the systems while maintaining working relationships with points of contacts monitoring data collection in the field. The following sections will provide details regarding panel selection, test system manufacturing and distribution, and analysis techniques. Due to the amount of detail and meticulous planning required for the research, mistakes were likely to occur and will be explained in this chapter as potential sources of error.

Test System Design, Manufacture, and Distribution

The primary targets of this study were two types of silicon-based PV panels: monocrystalline and polycrystalline. These panel types are commercially available off-the-shelf, which make them the most likely candidates for use in any given PV application. Further research may concern itself with thin-film PV or other emerging technologies. These crystalline panels produce the same amount of electricity per rated watt, although monocrystalline is slightly more space efficient. For the sake of thoroughness, both types are included to ascertain any differences in the effects of temperature and humidity between the two types. For each test system, one 50W polycrystalline panel and one 25W monocrystalline panel are included.

Each control unit, as shown in Figure 14, is equipped with a temperature/humidity probe to collect measurements of primary factors, a satellite communications uplink, and a central processing unit (CPU) for central control of peripheral devices. Sensitive electronic equipment is protected from the elements within a robust Pelican™ case. Panels are equipped with power-monitoring circuits shown in Figure 15. These devices transmit data via a CAT5e network cable to the CPU for storage.

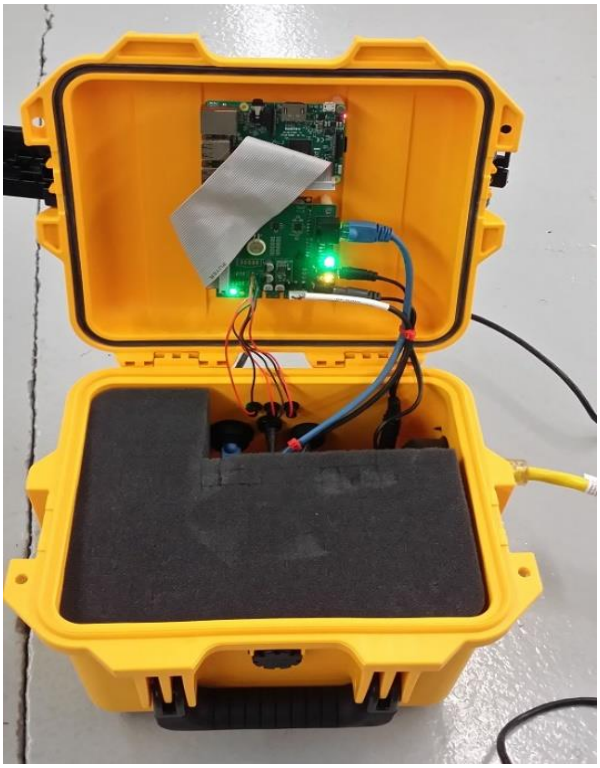

Figure 14. Control unit housing

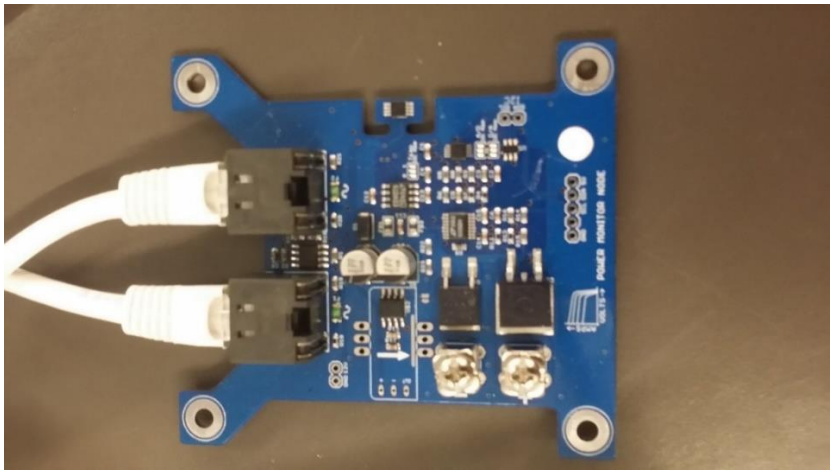

Figure 15. Power-monitoring circuit

Ambient temperature, humidity, and power output measurements are made every 15 minutes and contain 64 distinct voltage and current readings within each interval. Each measurement is then stored on a Micro SD flash memory card for later retrieval and submission to researchers. Additionally, data submissions are requested to be ideally made at the end of each month to maintain a steady influx of data for compilation for future analysis. The CPU used for this system is a Raspberry Pi, displayed in Figure 16, which is a standard operating computer containing typical components such as random access memory (RAM), graphics processing unit, and peripheral connections (Maksimovic & Vujovic, 2014). The CPU interface is conducted using a standard keyboard for command entry and display monitor. Figure 17 shows the different available components such as SD flash memory card port, USB, Local Area Network (LAN) connection, audio/video capability (HDMI included), and LED status indicators.

Figure 16. Raspberry Pi (Maksimovic & Vujovic, 2014)

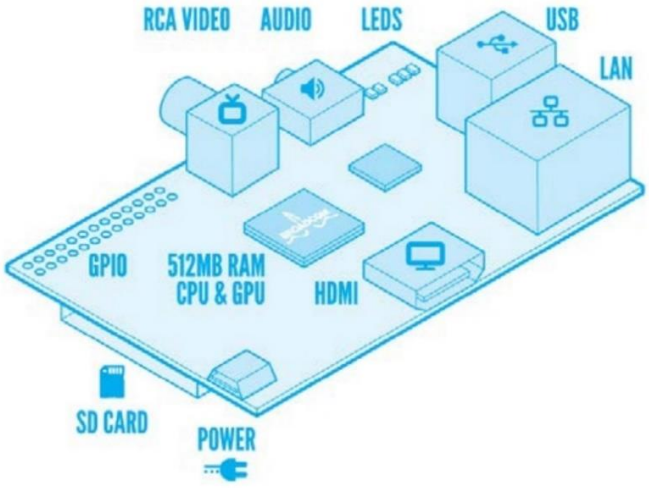

Figure 17. Raspberry Pi Components (Maksimovic & Vujovic, 2014)

Attached to each CPU is a RockBlock MK2 Iridium Satellite uplink capable of sending and receiving short messages from anywhere on earth (Rock Seven, 2014). The RockBlock unit is shown in Figure 18. Each system is programmed to transmit a daily system health update to ensure system operation and stability using the 18-digit coded message shown in Figure 19. Note that each message provides nine data points serving a

specific purpose to allow researchers to verify system status. In order, they are mean ambient temperature in degrees Celsius, mean ambient humidity, average daily power produced by each panel, operating voltages on both panels, panel node temperatures, and motherboard temperature.

Figure 18. RockBlock MK2 (Rock Seven, 2014)

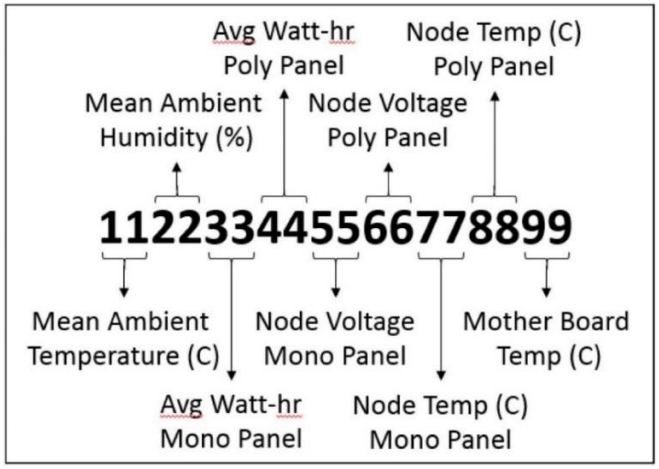

Figure 19. System health update (Nussbaum, 2017)

The control units are not self-powered and require an external 110-240V, 50-60 Hz power source for operation. Sites are required to connect their respective unit to a prime power source or use a standalone battery provided by researchers prior to the start of the study. Five of the 37 test sites required a battery as a power source due to limitations in authorized placement locations for the systems combined with lack of available prime power source. The chosen battery type and accompanying control unit is a 12V, 12ah, sealed lead acid battery purchased from AA Portable Power Corporation. These units come equipped with a DC control unit and provide a stable DC power source for the test system. The battery and DC controller are displayed in Figures 20 and 21. They are recharged via an additional 30W mono-crystalline PV panel. A complete system set-up with battery power source and charging PV panel is displayed in Figure 22.

Figure 20. 12V 12Ah battery with DC controller (AA Portable Power Corp, 2017)

Figure 21. 12V battery DC control unit (AA Portable Power Corp, 2017)

.

Figure 22. Complete test system with battery and charging panel

Methods of Analysis

The following sections discuss the methods used to analyze the data gathered from the PV test systems spread around the globe. The first method, multivariate linear regression, attempts to fit a performance model to the given data. The second method is a two-sample t-test and is used to determine whether the means of two samples are significantly different. Further detail is provided in the following sections.

Multivariate Linear Regression

The primary method of analysis applied to garnered data is multiple linear regression, a method used to ascertain statistically significant relationships between multiple variables. This method is used in this study to characterize power output as a function of temperature and humidity, producing performance models that describe variable effects. An example of these results is shown in Figure 23. A simple linear regression considers a single independent variable to predict the dependent variable and is generally described by the following equation, where b_n are regression coefficients:

$$Y = b_0 + b_1 x$$

Multiple regression expands on the simple expression by including the additional factors:

$$Y = b_0 + b_1 x_1 + b_2 x_2 \ldots + b_n x_n$$

Even more generally, multiple regression models often include representations of the interactions between variables and the random error, ε, associated with each observation (Statistics How To, 2018). These effects are described by the following general model:

$$Y = b_0 + b_1 x_1 + b_2 x_2 + b_{12} x_1 x_2 \ldots + b_{nm} x_n x_m + \varepsilon$$

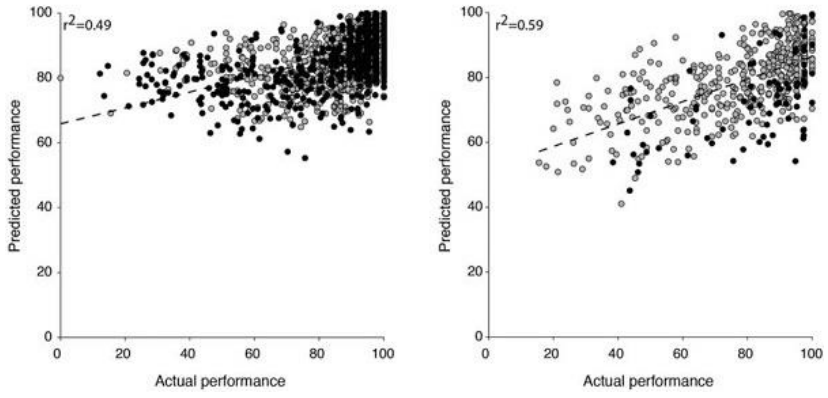

Figure 23. Linear regression output example

The aim is to model each panel type separately with power output being the sole dependent variable in their respective models. Since the two panel types are of different sizes, the polycrystalline panel being double the size of the monocrystalline, each power output reading was converted into wattage per square foot of area. The independent variables considered are the month, season, latitude, longitude, humidity, ambient temperature, internal control system temperature, and respective node temperatures. Also included is a factor indicating daylight hours for the purpose of excluding night data from the analysis. This factor is calculated from sunrise and sunset data obtainable from the website owned by the Astronomical Applications Department of the U.S. Naval Observatory (Astronomical Applications Department, 2016). As a reminder, a node consists of a PV panel and its attached power-monitoring circuit. Interactions between independent variables may result in collinearity, which is typically a disqualifier for inclusion. Multivariate regression assumes the absence of this effect, along with a few other key assumptions (Statistics Solutions, 2018).

The first assumption required to conduct a multivariate regression is a linear or curvilinear relationship between variables which can be observed using scatterplots. Second, multivariate normality is assumed to ensure residuals of the regression follow a normal distribution. Histograms or goodness of fit tests (Kolmogorov-Smirnov, Shapiro-Wilks, etc.) can be used to assess normality. The third assumption is lack of multicollinearity, which occurs when independent variables are highly correlated with each other. These can obscure principle components that explain variance in dependent variable observations and should be filtered out. The final assumption is

homoscedasticity of the data, which indicates error variances are similar across independent variables and can be checked for using a scatterplot of residuals against predicted values. Non-equal distribution of residuals indicates heteroscedasticity and would necessitate a non-linear transformation, introduction of a quadratic term, or other remedial technique to aid analysis. Verifying the key assumptions allows the application of multivariate linear regression. Multiple models are likely required to account for differing panel types, latitudes, or other unforeseen variables. Further, test site monitors may place their systems on different surfaces and at varying elevations. To control for these possible discrepancies, multiple test systems are placed in the same location, within one mile of each other, to collect measurements for variance testing.

Variance Testing

Testing for variance using three or more systems, as originally planned, would requires an analysis of variance (ANOVA) to check for significant variation between outputs from multiple systems. However, due to system error on one of the home systems, only two of the systems are analyzed to ascertain variance in differing surfaces. Therefore, a two-sample t-test is conducted to determine any significant difference in the independent sample means. This process ensures any variance in power output between the differing surface types has minimal interference with the temperature/humidity study. The two independent samples being examined are from a ground-level pavement surface and a rooftop system. Follow-on research will attempt to ensure all three systems are functional for a thorough variance test. A two-sample t-test sample output using JMP statistical analysis software is shown in Figure 24. Significant deviations between the

outputs show that repeat testing is needed at more than two locations at varying elevations and surface types or that performance models should include these factors as predictive variables.

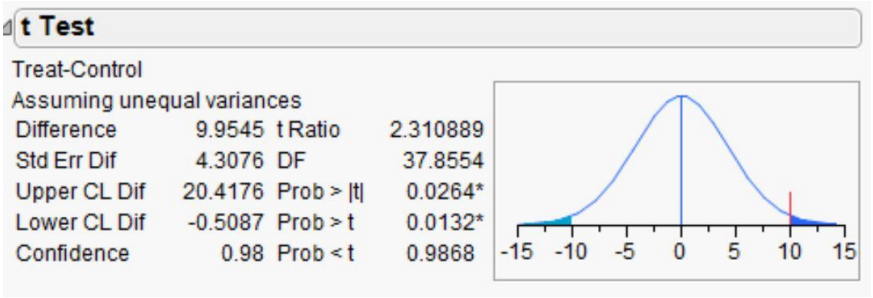

Figure 24. Example two-sample t-test results using JMP software

Potential Sources of Error

Working with commander-appointed test site monitors at each of the 37 testing locations presents a unique set of challenges, as each installation has their own priorities and mission sets which may compete which the collection of research data. Because of this, timing may not line up as desired with respect to start times; submission dates; gaps in data due to outages, system errors, etc.; or other contingencies.

DoD's prohibition of flash memory on government-owned networks presents another challenge for test sites. Since the control units utilize flash memory for storage of PV measurements, system monitors will need to retrieve data using other methods. Teammates may be required to seek approval from installation communications authorities to retrieve and transmit the data through the communications unit or to use pre-approved flash devices. The use of personal computers with SD card readers is encouraged, as it has proven to be the simplest method as it bypasses the need for vetting by communications authorities.

IV. ANALYSIS AND RESULTS

The aim of this chapter is to perform all necessary analysis to obtain an accurate performance model characterizing the behavior of monocrystalline and polycrystalline photovoltaic (PV) panels in each zone enumerated in Table 2. The test zone identification process discussed in the previous chapter allowed for selection of U.S. military installations and appointment of site monitors to install, monitor, and transmit data from their respective test systems. This chapter begins with an explanation of the amount and quality of data garnered from installations participating in the study and then breaks down the results of relevant analyses. First, global models are sought that predict behavior across the earth. New models are then obtained for four of the five existing Köppen climate types. As a reminder, this is because the Air Force does not operate in polar climate, thus there are no available test sites. Finally, site-specific expressions are provided to identify regions where ambient temperature and humidity have the most effect on power output. The chapter concludes with comparisons of resulting models with existing performance models discussed in the review of the literature.

Data Quality

Power performance data was obtained from 25 of the 37 test locations. Those sites that were not able to transmit data faced various issues with priority, setup, systems errors, or availability of power. All test locations are shown in Table 5, which is analogous with Table 2. In addition, Table 6 lists each participating location and its respective Köppen climate type.

Table 5. Test Site participation

Region	Actual Latitude	Actual Longitude	Site Name	Owning Installation of Record
A	20.890247	-156.4447	KAHULUI COMMUNICATION STATION	KEAUKAHA MIL RESERVATION
C	12.187654	-68.970935	CURACAO SITE # 1 - Aruba	DAVIS MONTHAN AFB
D	11.5183	43.0672	CHABELLEY	USAFE-AFAFRICA
E	-22.219846	114.103057	LEARMONTH AF SOLAR OBSERVATOI	YOKOTA AB
G	32.8888	-106.1038	HOLLOMAN SITE # 1	HOLLOMAN
G	29.12	-100.48	LAUGHLIN AFB AUX 1 SITE # 1	LAUGHLIN AIR FORCE BASE
G	34.39	-103.32	CANNON AFB SITE # 1	CANNON AIR FORCE BASE
G	33.904322	-117.262814	MARCH AFB SITE # 1	MARCH AIR RESERVE BASE
H	31.1833	-92.632	CLAIBORNE AIR FORCE RANGE SITE #	BARKSDALE AIR FORCE BASE
H	26.983	-80.108	JONATHAN DICKINSON MISSILE TRAC	PATRICK
I	34.5901	32.9892	RAF AKROTIRI	RAF AKROTIRI
J	33.581778	130.448329	ITAZUKE AUXILIARY AIRFIELD SITE #	YOKOTA AB
L	41.0508	-112.9356	UTTR - NORTH SITE # 1	HILL AFB
L	41.13	-95.75	OFFUTT FAMILY HOUSING ANNEX SIT	OFFUTTAIRFORCEBASE
L	38.16	-121.56	TRAVIS ILS OUTER MARKER ANNEX S	TRAVIS AFB
L	38.82	-104.71	PETERSON AFB SITE # 1	PETERSON AFB
L	38.95	-104.83	U S A F ACADEMY SITE # 1	U S A F ACADEMY
L	41.1517	-111.9922	SO WEBER ENVIRONMENTAL ANNEX	HILL AFB
M	40.66807	-86.14765	GRISSOM AIR FORCE BASE SITE # 1	GRISSOM ARB
M	37.08	-76.37	LANGLEY AFB SITE # 1	JBLE
M	40.026986	-74.584263	MCGUIRE AFB	JB MDL
M	44.89	-93.2	MINN-ST PAUL SITE # 1	MINN-ST PAUL
N	38.7754	-27.0891	LAJES FIELD SITE # 1	LAJES FIELD
O	37.753755	127.027811	CAMP RED CLOUD COMMUNICATION	OSAN
O	37.08	128.59	OSAN SITE # 1	OSAN AB
P	55.245335	-162.770084	COLD BAY LONG RANGE RADAR SITE	EARECKSON AS
Q	47.7947385	-101.2979626	MINOT AF MISSILE SITE D1 SITE # 1	MINOT AFB
Q	47.11439	-122.573129	CAMP MURRAY AGS SITE # 1	CAMP MURRAY AGS
Q	48.418476	-101.338604	MINOT AFB SITE #1	MINOT AFB
Q	47.52	-111.18	MALMSTROM SITE # 1	MALMSTROM AFB, MT
R	46.933892	-67.911875	DFAS ANNEX - Limestone Maine	WHITEMAN
S	50.0166	6.7704	GROSSLITTGEN WATER SYSTEM ANN	SPANGDAHLEM
T	52.729239	174.099627	EARECKSON AS SITE # 1	EARECKSON AS
U	64.2852	-149.1515	CLEAR AIR FORCE STATION SITE # 1	CLEAR AIR FORCE STATION
U	65.564961	-167.967703	TIN CITY LONG RANGE RADAR SITE	EARECKSON AS
W	76.53	-68.7	THULE AIR BASE SITE # 1	THULE AIR BASE
X	58.905625	5.7215649	STAVANGER ADMIN OFFICE SITE # 1	RAF ALCONBURY

Table 6. Analyzed test locations and their corresponding Köppen climate types

Climate Types by Location

Location	Koppen Climate	Location	Koppen Climate
Camp Murray, WA	Temperate	Lajes, PT	Temperate
Camp Red Cloud, KR	Boreal	Langley AFB, VA	Temperate
Chabelley, DJ	Dry	Learmonth Solar Obs, AU	Dry
Curacao, AW	Tropical	Malmstrom, MT	Dry
DFAS Annex, IN	Boreal	March ARB, CA	Temperate
Grissom, IN	Boreal	Minnasota ANG, MN	Boreal
Grosslittgen, DE	Temperate	Offutt, NE	Boreal
Hill UTTR, UT	Boreal	Peterson, CO	Boreal
Hill Weber Annex, UT	Boreal	RAF Akrotiri, CY	Temperate
Holloman, NM	Dry	Travis AFB, CA	Temperate
Johnathan Dickinson, FL	Tropical	USAF Academy, CO	Boreal
Kahului, HI	Tropical		

Note that data garnered from installations are highlighted in green. Several locations were able to install and begin data transmissions as early as May, 2017. Of the locations that submitted data, the latest test start date covered the month of October, 2017. As of this writing, these 25 systems are still operating. They will continue the study into the following year with the other 12 test sites working to address various technical or installation issues including battery malfunction, component failure, faulty data, or anchoring system problems. All test systems, with the exception of three systems sent to the Alaskan zone installations, were confirmed by site monitors as received and intact. These are expected to join the study early in 2018. Inclusion of more systems into the study will yield more data and hone the accuracy of resulting performance models.

Performance Modeling

Multiple linear regression was performed using JMP Pro Statistical Analysis Software, Version 12.0.1, 64-bit edition by SAS Institute Inc. The aim was to characterize each panel type separately as the difference in material type may be influenced by environmental factors in unforeseen ways. Fitting the data to a linear model requires testing the key assumptions for multivariate linear regression outlined in chapter III to ascertain whether non-linear analysis techniques or transforms are necessary. A best model for each panel type is then selected that allows a reasonable prediction of energy output at locations with wide distributions of temperature and humidity. Varying accuracy prompted additional models applicable to respective climate types and specific locations around the world. The effect each predictor had on the power output and coefficient of determination (R^2) accuracy depends heavily on the

location, alluding to a high probability of additional location or region-specific predictors affecting the power output of PV panels. Following initial experimentation with global models, a new factor was introduced to delineate between the five Köppen climate types (tropical, dry, temperate, boreal, and polar) and enable the creation of new models that pertain to each climate type and provide more accurate characterization. Note that in some models, the response variable is the logarithm of power output. In an effort to improve the models and account for additional variance, Y and X value transformations were used to linearize the models, create constant variance in the plot of residuals against predicted values, and create a linear relationship with predictor variables. The five transformations listed in Table 7 were used on response and predictor variables to find the best fitting model. The best result for all models used a square root, logarithmic, or no transform to linearize Y-values. Finally, multiple regression assumes that the independent variables are not highly correlated with each other. This assumption is tested using Variance Inflation Factor (VIF) values. As a general rule, VIFs greater than 10 indicate problematic collinearity between variables (Statistics Solutions, 2018).

Table 7. Transformations of Y to improve model performance (Buro, 2018)

Relationship between the error variance and the mean response	Transformation of Y
$\sigma^2 \propto E(Y)$	square root
$\sigma^2 \propto E(Y)^2$	log
$\sigma^2 \propto E(Y)^3$	reciprocal square root $(1/\sqrt{(y)})$
$\sigma^2 \propto E(Y)^4$	reciprocal
$\sigma^2 \propto E(Y)(1 - E(Y))$	if $0 \leq Y \leq 1$, arcsin, $(sin^{-1}(\sqrt{(y)})$

Key Assumptions

Confirmation of model validity is first tested on the performance of the monocrystalline panels, followed by the polycrystalline panel. A linear relationship should be shown between each panel type and the independent variables. The scatterplots for select locations in Figure 25 show one-to-one relationships between power output and the independent variables of ambient temperature and humidity. It can be seen from the scatterplots that knowledge of these factors alone does not allow an accurate prediction of power output. Regardless, there is indication of a positive trend for ambient temperature while humidity shows a negative trend. Interactions with other factors likely explain the remaining variance in observations. Similar relationships are shown for polycrystalline panel performance in Figure 26, though it appears the independent variables are more correlated with power output for this material type.

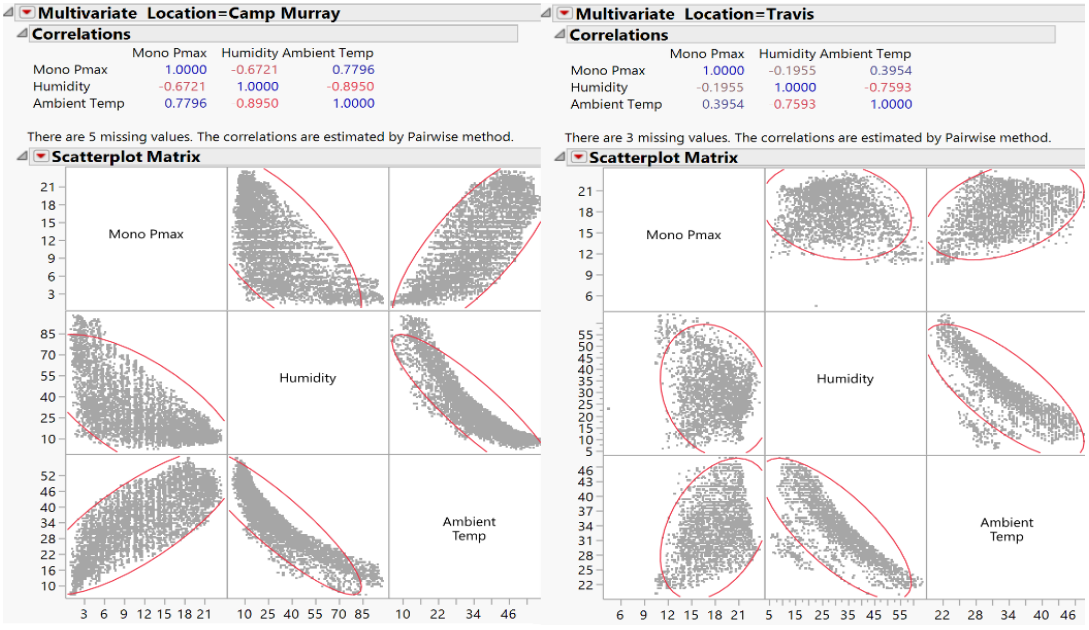

Figure 25. Monocrystalline correlations at select locations, strong and weak examples

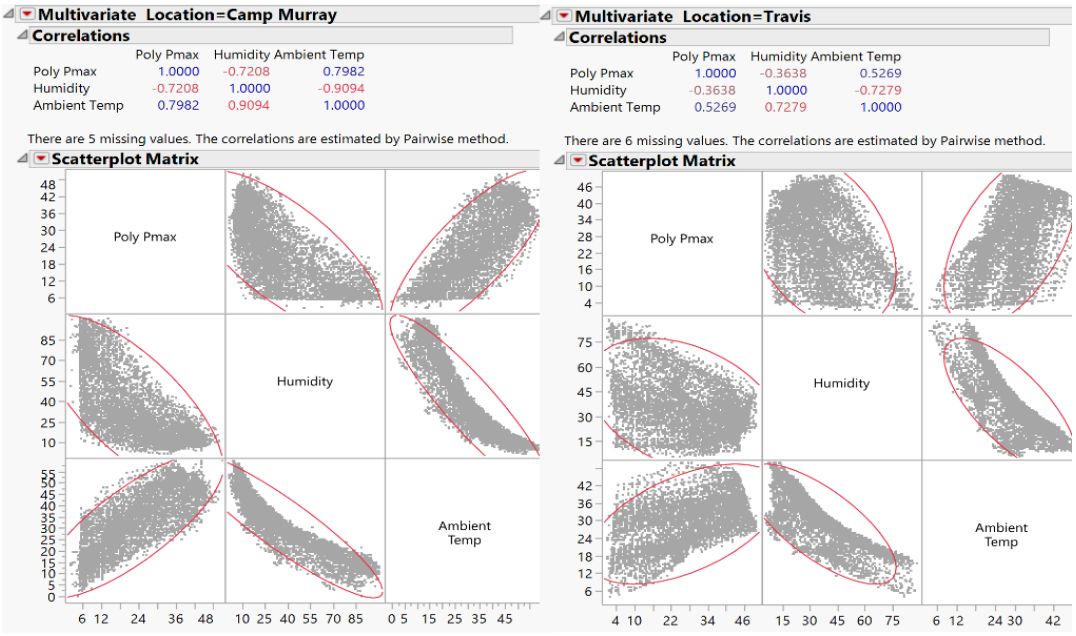

Figure 26. Polycrystalline correlations at select locations, strong and weak examples

Monocrystalline Models

The first model attempted to characterize temperature and humidity across all ranges of latitude and longitude. Key assumptions for linearity were met, though the result was unsatisfactory with an R^2 value of 0.3111, indicating that only 31.11% of the variation in the response is explained by the presence of these predictive variables. The dependent variable y describes the power output in watts(W), L_t is the latitude, L_n is the longitude, t is the ambient temperature, and h is the humidity. The global performance model for monocrystalline PV panels is described by the following:

$$\ln y = 0.012L_t - 0.004L_n + 0.015t + 0.003(L_t - 40.691)(t - 32.77)$$
$$+ 0.001(h - 36.059)(t - 32.77) + 0.465$$

Goodness-of fit tests can be conducted. However, due to such large sample sizes, there is great sensitivity in tests for normality and failing them does not necessarily mean a linear model cannot be created (Ghasemi & Zahediasl, 2012). A visual inspection of the residual distribution histogram confirms the data is approximately normal and analysis can continue unabated. Validity of the model and the linear relationship with predictor variables are seen are seen in Figures 27 (top right) and 28, respectively. In addition, the resulting VIF values indicate no issues with collinearity among the predictor variables. The low R^2 value may not be accurate enough to base decisions on, but it is significant enough that the predictors should definitely be kept and supplemented with additional predictors to hone accuracy. The histogram in Figure 27 shows underestimations for the majority of predictions and overestimates concentrated in a specific small range. This spike in overestimates may stem from location or region-specific conditions. Location-dependent model accuracy, discussed in a later section, confirms that residual values are expected to concentrate in different areas of the histogram. In addition, linearity with predictor variables was vastly improved by using a logarithmic data transformation compared to the non-transformed, cone-shaped values in Figure 29. Subsequent performance models are provided without the full analyses in this chapter. For the analyses of remaining global and climate-based models, comparable to the one provided in Figures 27 and 28, see the appendix.

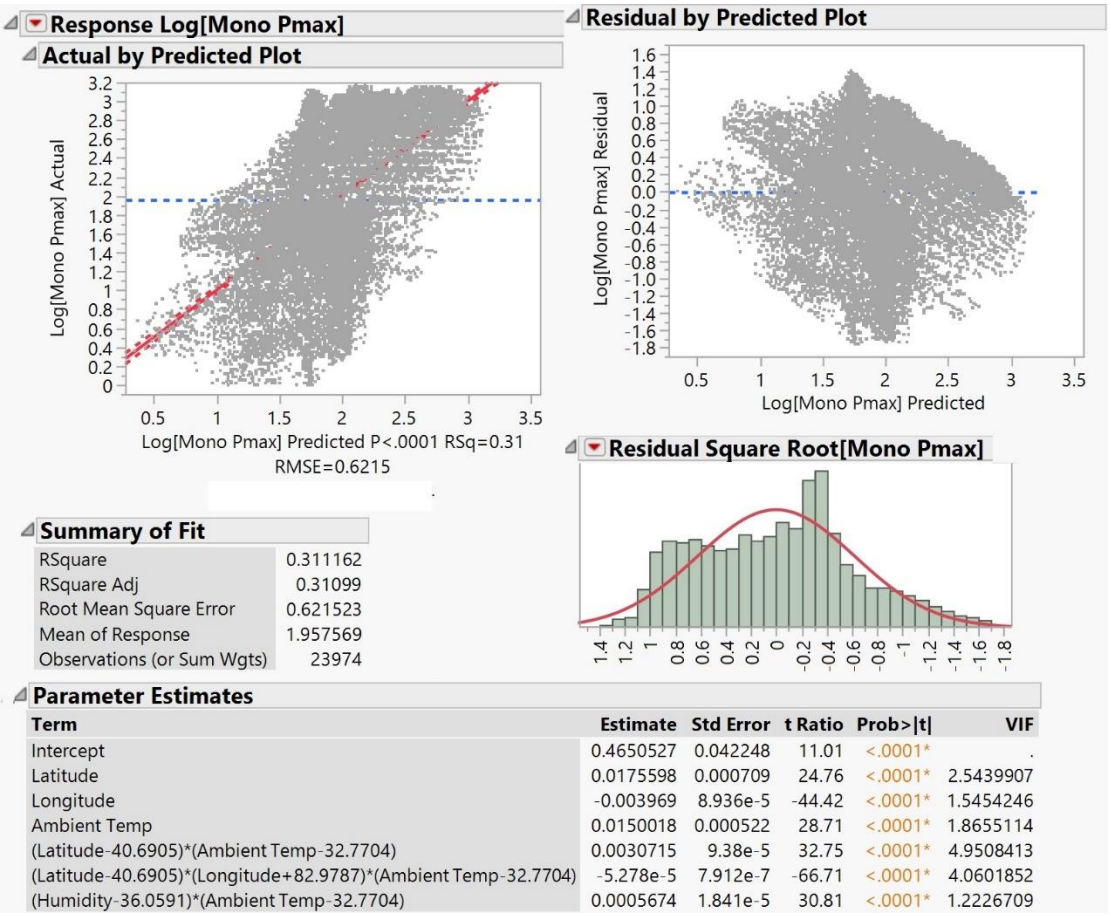

Figure 27. Monocrystalline global model, $R^2 = 0.3111$

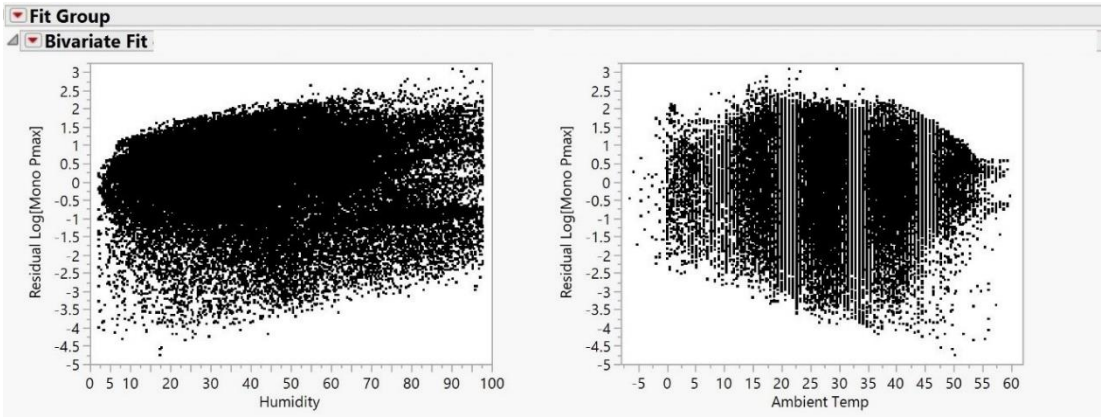

Figure 28. Post-transformation residual plots with predictors indicating linearity

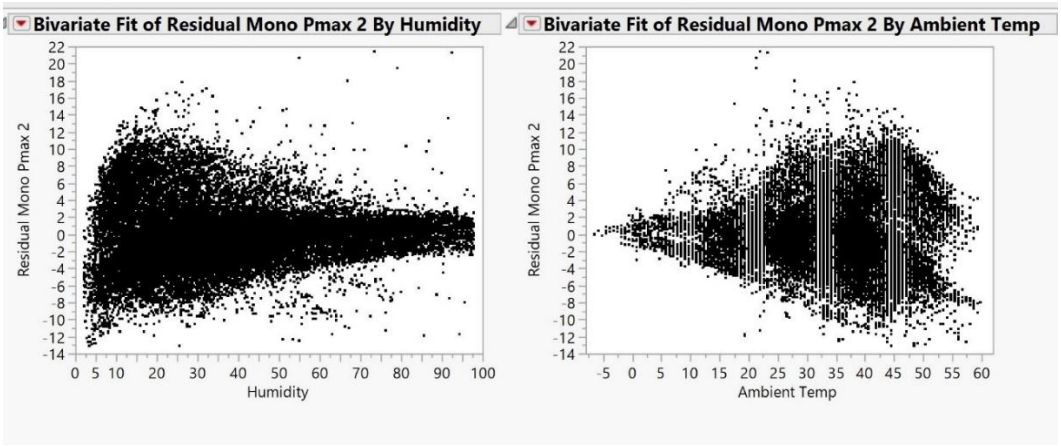

Figure 29. Cone-shaped residual pattern indicating non-linearity

The boreal climate type is the first of the four climate types in which a model is built. Experimentation with transformation functions from Table 7 and observance of model diagnostics indicate a logarithmic Y-transform is the most appropriate, yielding the highest correlations with ambient temperature and humidity. The power output in boreal climate is described by the following equation:

$$\ln y = 0.229L_t - 0.028L_n - 0.006(L_t - 42.306)(L_n + 90.423) + 0.019t + 0.0003(L_n + 90.423)(t - 33.283) + 0.00007(L_t - 42.306)(h - 31.724)(t - 33.283) - 11.293$$

The result shows a significant predictive relationship between predictors and power output for this climate type with an R^2 value of 0.6120. The dominant variables are latitude; longitude; ambient temperature; humidity; and interactions between latitude and longitude, longitude and temperature, and latitude with humidity and temperature. The clustering seen occurring on the plot of observed versus predicted values correspond

to different test locations, a predictable result given the various R^2 accuracies among locations. Similar results are seen in the residual histogram. Effects of individual predictors are better seen in the location-specific models, though significance of coordinate effects indicate missing predictor variables that describe local or regional site conditions needed to obtain performance model accuracy.

The next climate type test is dry climate. The Y-transform used for linearizing dry climate types outputs is the square root of the dependent variable. The power output for monocrystalline PV in the dry climate type is given by the following:

$$\sqrt{y} = -0.002L_n - 0.006(L_t - 27.673)(L_n + 28.359) + 0.002(L_t - 27.673)(h - 20.757) + 0.05t - 0.0002(L_n + 28.359)(t - 39.006) - 0.527$$

Obtaining any accuracy with this particular model was difficult as was correcting linearity by applying a square root transform. The equation describing dry climates, with an R^2 value of 0.3044 and a tendency to underestimate power output predictions, contains environmental factors not explicitly identified but encapsulated by changes in latitude and longitude. These unknown components are seen interacting with ambient temperature and humidity. The resulting bivariate graphs show a linear relationship is maintained between power output and the independent variables.

The temperate climate model utilizes the same data transform as the dry climate model and acheives a slightly greater accuracy with an R^2 value of 0.4109. The power equation is as follows:

$$\sqrt{y} = 0.0006(L_t - 43.048)(L_n + 90.666) + 0.002(L_t - 43.048)(h - 37.108) + 0.021t - 0.015(L_t - 43.048)(t - 32.616) + 0.0001(L_t - 43.048)(h - 37.108)(t - 32616) + 2.673$$

Variation in power output appears to be relatively even between all locations encompassed by the temperate category, evidenced by the lack of clustering and relatively even number of residuals on either side of the best fit line.

The final climate model is tropical. It was found that a logarithmic transform yielded the greatest accuracy for tropical climates, unlike, dry, and temperate. Accuracy is second highest to the boreal model with an R^2 value of 0.5472. The power output is given by the following equation:

$$\ln y = -0.422L_n - 13.977\ln h - 13.18 \ln t + 0.118(L_n + 76.153) \ln t + 3.69 \ln h \ln t + 19.253$$

Significant clustering on the residuals histogram is evident, showing differences in specific locations that affect accuracy along with a more severe tendency to underestimate power predictions. The bivariate fit at the bottom of the figure, with exception of a few data points, maintains that there is linear relationship between power and the predictor variables of interest, temperature and humidity. It is thought that inclusion of additional factors, to be discussed in more detail during researcher recommendations, will help refine each model's accuracy.

Polycrystalline Models

The following models describe the effects of ambient temperature and humidity using polycrystalline PV panels. The same analyses are again conducted, first attempted for a global characterization and then on the four Köppen climate types. Polycrystalline material appears to behave slightly differently, requiring different data transforms to obtain the most accurate models. The global model utilized a square root transform, though validity is highly suspect with an R^2 value of 0.2166. The global power output is given by the following equation:

$$\sqrt{y} = -0.004h + 0.05t + 0.0002(h - 39.096)(t - 31.745) + 0.01L_t + 0.002L_n + 2.035$$

Additional factors are definitely necessary to refine this model. The boreal, tropical, and dry models all used the square root transform as it was more accurate than the logarithm. The respective power equations for the boreal, tropical, and dry climate types are as follows:

$$\sqrt{y} = -0.007h + 0.047t - 0.0001(h - 30.702)(L_n + 89.757) - 0.003(L_t - 40.779)(L_n + 89.757) + 0.141L_t - 0.005L_n - 4.263$$

$$\sqrt{y} = 0.167t - 0.513(L_t - 20.369)(L_n + 87.437) - 0.004(L_t - 20.369)(t - 35.627) + 0.0005(L_n + 87.437)(h - 56.021) - 0.016h + 6.95L_t - 163.981$$

$$\sqrt{y} = 0.083t + 0.0006(L_t - 14.801)(t - 32.712) + 0.0005(t - 32.712)(h - 27.901) - 0.0003(L_t - 14.801)(L_n + 3.765) + 0.071L_t + 0.015L_n - 0.47$$

Resulting accuracies were less reliable than monocrystalline models for boreal and tropical climates but more accurate for dry climate with R^2 values of 0.3999, 0.5210, and 0.3956, respectively. Seemingly non-linear bivariate plots for dry climate type may be the result of total non-validity of the derived model. However, it may also be the result of superimposing residuals from multiple locations with differing model accuracy. This type of clustering was also seen in previous models, especially that of the boreal climate using a monocrystalline panel. Temperate climate required a logarithmic transform and yielded an R^2 value of 0.3693. The equation for the temperate climate models is as follows:

$$\ln y = 0.044L_t - 0.006h + 0.028t + 0.0002(L_t - 40.886)(L_n + 78.237) + 0.0003(h - 44.147)(t - 29.793) - 0.0003L_n + 0.42$$

Clustering of residuals for the temperate climate is also especially apparent, indicating significant environmental differences between temperate test sites. Again, it is apparent that additional, currently unidentified predictors are necessary to further refine these models. However, the coefficients are significant enough that interactions between ambient temperature and humidity should definitely be included in all models.

Regression Models by Location

Significant inaccuracies are apparent in the global and climate-specific regression models. Therefore, it is necessary to ascertain the effects of temperature and humidity at each test location by modeling power output from each test system. The intent is to reveal the best and worst fit models described by these predictors. Table 8 lists location-specific regression equations, their R^2 values, and predictor effects summary for monocrystalline panels. The same information is provided for polycrystalline panels in Table 9. There may be some test sites in which information is incomplete or missing. In these cases, the model fit (R^2 value) was too low to provide any worthwhile result. In these cases, additional data will be required for future analysis.

LogWorth values describe predictor significance in each model. Values greater than 2 are considered significant with 99% confidence (0.01 level) and are derived from the following equation:

$$-\log_{10}(0.01) = 2$$

With respect to monocrystalline panels, the highest R^2 values were found at Hill AFB, Utah, at 0.8087 and Holloman AFB, New Mexico, at 0.8059. The resulting regression equations can be reasonably relied upon to forecast power production at these locations. There are other locations with reasonably accurate models such as Jonathan Dickinson missile tracking site, Florida (R^2=0.6510), Camp Murray, Washington (R^2=0.6415), and Grissom ARB, Indiana (R^2=0.6172). It can be seen from the predictor effects summaries that ambient temperature is a far more significant predictor than

humidity, though both are considered statistically significant enough to include in the models, as denoted by the LogWorth values.

Similar results are seen with polycrystalline panels, with some exceptions. The data gathered from the Air National Guard installation in Minnesota shows humidity was a significant factor for only monocrystalline panels and not for polycrystalline. Another point of interest is data from the sole test location in the southern hemisphere. The least accurate model came from Learmonth Solar Observatory with R^2=0.1076, indicating the resultant model does not fit the data. This may indicate factors unique to the southern hemisphere that affect solar irradiance and warrant additional research. Lastly, only RAF Akrotiri data indicated that the interaction between temperature and humidity had a greater effect on power than temperature alone for both panel types.

Table 8. Monocrystalline regression models and predictor effects by location

Panel type: monocrystalline

Location	Model Expression	R Sq	Predictor Effects
Camp Murray, WA	$(-0.0806686104518 + 0.01321073988221 * \text{Humidity} + 0.08732904426554 * \text{Ambient Temp} + (\text{Humidity} - 30.7206697160121) * ((\text{Ambient Temp} - 34.3209246364552) * 0.00050380994663))^2$	0.6415	Source / LogWorth: Ambient Temp 333.957; Humidity*Ambient Temp 25.161; Humidity 23.607
Camp Red Cloud, KR	$\text{Exp}(-0.2093214883921 + -0.013177520281 * \text{Humidity} + 0.05054460601805 * \text{Ambient Temp} + (\text{Humidity} - 36.1208063377193) * ((\text{Ambient Temp} - 39.2126400438597) * 0.0025241743005))$	0.3039	Source / LogWorth: Ambient Temp 8.781; Humidity*Ambient Temp 3.239; Humidity 2.163
Chabelley, DJ	Unavailable	N/A	N/A
Curacao, AW	$\text{Exp}(0.03559288231422 + -0.0168068377204 * \text{Humidity} + 0.05650392816256 * \text{Ambient Temp} + (\text{Humidity} - 49.4606633157895) * ((\text{Ambient Temp} - 39.0724516491228) * 0.00324635618838))$	0.4340	Source / LogWorth: Humidity*Ambient Temp 10.448; Ambient Temp 3.188; Humidity 2.189
DFAS Annex, IN	$(1.64565878337344 + -0.0078133581411 * \text{Humidity} + 0.01327061011807 * \text{Ambient Temp} + (\text{Humidity} - 38.4112268496732) * ((\text{Ambient Temp} - 24.8938424313726) * -0.0003341885908))^2$	0.3116	Source / LogWorth: Ambient Temp 36.318; Humidity 24.028; Humidity*Ambient Temp 8.954
Grissom, IN	$(0.7879757824928 + -0.0081014693347 * \text{Humidity} + 0.04108703634459 * \text{Ambient Temp} + (\text{Humidity} - 38.1887212768496) * ((\text{Ambient Temp} - 34.296248353222) * -0.0004613424249))^2$	0.6172	Source / LogWorth: Ambient Temp 56.865; Humidity 12.877; Humidity*Ambient Temp 5.281
Grosslittgen, DE	$6.34413938262541 + -0.1058934129198 * \text{Humidity} + 0.37342812887044 * \text{Ambient Temp} + (\text{Humidity} - 66.3058520718697) * ((\text{Ambient Temp} - 21.7082112521056) * -0.0109876015708)$	0.4449	Source / LogWorth: Ambient Temp 31.419; Humidity*Ambient Temp 20.668; Humidity 19.419
Hill UTTR, UT	Unavailable	N/A	
Hill Weber Annex, UT	$\text{Exp}(1.39908876386233 + 0.00214343289248 * \text{Humidity} + 0.00941463517748 * \text{Ambient Temp} + (\text{Humidity} - 23.3388048351044) * ((\text{Ambient Temp} - 34.7836345218029) * 0.00008131772605))$	0.8087	Source / LogWorth: Ambient Temp 873.097; Humidity*Ambient Temp 75.638; Humidity 56.656
Holloman, NM	$\text{Exp}(-2.8422963108497 + 0.13307431163378 * \text{Ambient Temp} + (\text{Humidity} - 31.2977969014084) * ((\text{Ambient Temp} - 29.4165045070423) * 0.00307983392245))$	0.8059	Source / LogWorth: Ambient Temp 24.390; Humidity*Ambient Temp 2.518

Jonathan Dickinson, FL	$\text{Exp}\left[\begin{array}{l}-3.1793481368744 \\ +\ -0.0061044686246 * \text{Humidity} \\ +\ 0.12701094564341 * \text{Ambient Temp} \\ \quad \{\text{Humidity} - 48.7446432089552\} \\ +\ * \left[\{\text{Ambient Temp} - 38.8119523283582\} * 0.00214224217173\right]\end{array}\right]$	0.6510	
Kahului, HI	Unavailable	N/A	N/A
Lajes, PT	$\text{Exp}\left[\begin{array}{l}1.8400751895487 \\ +\ -0.0051789326413 * \text{Humidity} \\ +\ 0.02849593649441 * \text{Ambient Temp} \\ \quad \{\text{Humidity} - 51.9027455673222\} \\ +\ * \left[\{\text{Ambient Temp} - 32.5891855673222\} * 0.00129418948523\right]\end{array}\right]$	0.2363	
Langley AFB, VA	Unavailable	N/A	N/A
Learmonth Solar Obs, AU	Unavailable	N/A	N/A
Malmstrom, MT	$\text{Exp}\left[\begin{array}{l}1.6381497121137 \\ +\ 0.03649257225526 * \text{Ambient Temp} \\ \quad \{\text{Humidity} - 18.8823797461929\} \\ +\ * \left[\{\text{Ambient Temp} - 30.4389188959391\} * 0.00285349307377\right]\end{array}\right]$	0.5861	
March ARB, CA	$\text{Exp}\left[\begin{array}{l}1.6381497121137 \\ +\ 0.03649257225526 * \text{Ambient Temp} \\ \quad \{\text{Humidity} - 18.8823797461929\} \\ +\ * \left[\{\text{Ambient Temp} - 30.4389188959391\} * 0.00285349307377\right]\end{array}\right]$	0.3603	
Minnasota ANG, MN	$\begin{array}{l}0.36971609530223 \\ +\ 0.38235257608132 * \text{Ambient Temp} \\ \quad \{\text{Humidity} - 46.6519583140569\} \\ +\ * \left[\{\text{Ambient Temp} - 30.581107566726\} * 0.0079607586968\right]\end{array}$	0.2528	
Offutt, NE	$\left[\begin{array}{l}2.70050863626801 \\ +\ -0.0159511144146 * \text{Humidity} \\ \quad \{\text{Humidity} - 42.4571809148265\} \\ +\ * \left[\{\text{Ambient Temp} - 31.7863475394322\} * 0.00124962052996\right]\end{array}\right]^2$	0.4612	
Peterson, CO	$\text{Exp}\left[\begin{array}{l}-0.3698911139653 \\ +\ -0.0239611175316 * \text{Humidity} \\ +\ 0.04226377699847 * \text{Ambient Temp}\end{array}\right]$	0.6007	
RAF Akrotiri, CY	$\text{Exp}\left[\begin{array}{l}-0.2263791390875 \\ +\ -0.0053021333928 * \text{Humidity} \\ +\ 0.05694535103048 * \text{Ambient Temp} \\ \quad \{\text{Humidity} - 38.0944364300626\} \\ +\ * \left[\{\text{Ambient Temp} - 37.6409068893529\} * 0.00330213832402\right]\end{array}\right]$	0.5465	
Travis AFB, CA	$\text{Exp}\left[\begin{array}{l}1.90355104729439 \\ +\ 0.0078784810951 * \text{Humidity} \\ +\ 0.02343630918578 * \text{Ambient Temp} \\ \quad \{\text{Humidity} - 30.5089993403909\} \\ +\ * \left[\{\text{Ambient Temp} - 33.3351019096091\} * 0.00083563618617\right]\end{array}\right]$	0.3117	

Table 9. Polycrystalline regression models and predictor effects by location

Panel type: polycrystalline

Location	Model Expression	R Sq	Predictor Effects
Camp Murray, WA	-1.8423085089489 + 0.75051757917938 * Ambient Temp + {Humidity - 37.640720354362} * {{Ambient Temp - 31.1497718576196} * -0.0011166215084}	0.6521	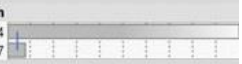
Camp Red Cloud, KR	Unavailable	N/A	N/A
Chabelley, DJ	Exp[-0.0586188198869 + 0.0689858239857 * Ambient Temp + {Humidity - 23.8979452045134} * {{Ambient Temp - 44.8014656981664} * 0.00231780679389}]	0.3267	
Curacao, AW	Exp[-2.3491451513441 + 0.13144926394057 * Ambient Temp + {Humidity - 55.5901930961232} * {{Ambient Temp - 36.8546623844928} * 0.00149849328713}]	0.5266	
DFAS Annex, IN	[4.00506858633481 + -0.0301868973745 * Humidity + 0.00938082540493 * Ambient Temp + {Humidity - 47.9465299339207} * {{Ambient Temp - 21.5964286894273} * -0.000866497342}]^2	0.4662	
Grissom, IN	2.84446905769797 + -0.0821988625842 * Humidity + 0.34618082442446 * Ambient Temp	0.4098	
Grosslittgen, DE	17.4757516048692 + -0.1728524979231 * Humidity + 0.55056535490442 * Ambient Temp + {Humidity - 76.3631947661971} * {{Ambient Temp - 18.0789493098591} * -0.0146531251284}	0.5460	
Hill UTTR, UT	[1.78492905328929 + -0.0134710684716 * Humidity + 0.05766504815241 * Ambient Temp + {Humidity - 17.3234580465116} * {{Ambient Temp - 27.6630663162791} * 0.00099129521763}]^2	0.6668	
Hill Weber Annex, UT	Exp[1.4584229391414 + 0.0070878305315 * Humidity + 0.0283707115656 * Ambient Temp + {Humidity - 17.5824189736788} * {{Ambient Temp - 39.236932071006} * 0.00114544843592}]	0.3752	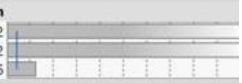
Holloman, NM	-33.137058436096 + 0.37124727664177 * Humidity + 1.20216680065392 * Ambient Temp + {Humidity - 20.4803305993691} * {{Ambient Temp - 34.7685450262881} * 0.03397529306131}	0.3731	
Johnathan Dickinson, FL	-18.182475247795 + -0.0974848548346 * Humidity + 1.07132364918447 * Ambient Temp + {Humidity - 54.3611345540631} * {{Ambient Temp - 36.6846076128606} * -0.0044208162482}	0.5573	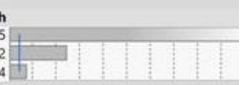
Kahului, HI	[0.95332058237398 + -0.0409425081836 * Humidity + 0.17066147799732 * Ambient Temp + {Humidity - 62.165605080537} * {{Ambient Temp - 29.3035048456376} * 0.00418080787264}]^2	0.3472	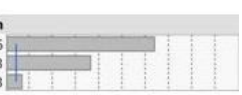

Lajes, PT	$\text{Exp}\left[\begin{array}{l} 2.08818764201514 \\ + -0.0095356301363 * \text{Humidity} \\ + 0.0344563968576 * \text{Ambient Temp} \\ + \left[\begin{array}{l}(\text{Humidity} - 66.1100388508946) \\ * \left[(\text{Ambient Temp} - 26.604674584493) * 0.00037487159434\right]\end{array}\right] \end{array}\right]$	0.3365	
Langley AFB, VA	$\text{Exp}\left[\begin{array}{l} 3.02205072568979 \\ + -0.0303863725955 * \text{Humidity} \\ + 0.01774419352469 * \text{Ambient Temp} \end{array}\right]$	0.355	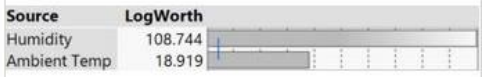
Learmonth Solar Obs, AU	$\text{Exp}\left[\begin{array}{l} 1.86214150576866 \\ + -0.0027772889377 * \text{Humidity} \\ + 0.02779517259642 * \text{Ambient Temp} \\ + \left[\begin{array}{l}(\text{Humidity} - 32.5512869319938) \\ * \left[(\text{Ambient Temp} - 35.9379548995363) * 0.00099105830894\right]\end{array}\right] \end{array}\right]$	0.1076	
Malmstrom, MT	$\begin{array}{l} 0.44989526133795 \\ + 0.05736745360966 * \text{Humidity} \\ + 0.73908268735722 * \text{Ambient Temp} \\ + \left[\begin{array}{l}(\text{Humidity} - 27.8342485185185) \\ * \left[(\text{Ambient Temp} - 22.4343743883277) * 0.0068396334527\right]\end{array}\right] \end{array}$	0.3896	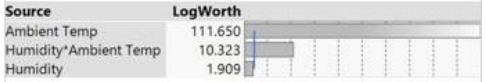
March ARB, CA	$\left[\begin{array}{l} 0.44830831325102 \\ + 0.08487283266517 * \text{Ambient Temp} \\ + \left[\begin{array}{l}(\text{Humidity} - 26.1482644440032) \\ * \left[(\text{Ambient Temp} - 34.447340420969) * 0.00111552985839\right]\end{array}\right] \end{array}\right]^2$	0.3239	
Minnasota ANG, MN	$\text{Exp}\left[\begin{array}{l} 1.66825653946459 \\ + -0.0033907972707 * \text{Humidity} \\ + 0.07080976372665 * \text{Ambient Temp} \end{array}\right]$	0.4103	
Offutt, NE	$\text{Exp}\left[\begin{array}{l} 1.26293144017121 \\ + 0.03211846877683 * \text{Ambient Temp} \\ + \left[\begin{array}{l}(\text{Humidity} - 42.7317440581129) \\ * \left[(\text{Ambient Temp} - 28.660894100555) * 0.00064560875484\right]\end{array}\right] \end{array}\right]$	0.2818	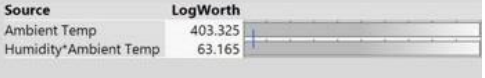
Peterson, CO	$\left[\begin{array}{l} 1.30761261388683 \\ + -0.020690989433 * \text{Humidity} \\ + 0.0532760557181 * \text{Ambient Temp} \\ + \left[\begin{array}{l}(\text{Humidity} - 18.4259518174619) \\ * \left[(\text{Ambient Temp} - 33.9047858839834) * -0.0007517055978\right]\end{array}\right] \end{array}\right]^2$	0.5248	
RAF Akrotiri, CY	$\text{Exp}\left[\begin{array}{l} 3.53321613692192 \\ + -0.0138128948213 * \text{Humidity} \\ + \left[\begin{array}{l}(\text{Humidity} - 35.0243559090909) \\ * \left[(\text{Ambient Temp} - 41.3997386818182) * 0.00250899009193\right]\end{array}\right] \end{array}\right]$	0.5915	
Travis AFB, CA	$\begin{array}{l} 0.46299435781845 \\ + 0.97064569219088 * \text{Ambient Temp} \\ + \left[\begin{array}{l}(\text{Humidity} - 37.5255404637516) \\ * \left[(\text{Ambient Temp} - 28.2830245466591) * 0.00864791689471\right]\end{array}\right] \end{array}$	0.3792	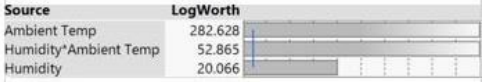
USAF Academy, CO	$\text{Exp}\left[\begin{array}{l} 1.50515640465821 \\ + 0.02575168910894 * \text{Ambient Temp} \\ + \left[\begin{array}{l}(\text{Humidity} - 29.3797488760807) \\ * \left[(\text{Ambient Temp} - 33.6748725600384) * 0.00028019359503\right]\end{array}\right] \end{array}\right]$	0.3407	

Model Coefficients

Predictors had similar effects for both panel types across global and climate type models. Observance of patterns in the data show an increase in power output commensurate with movement west of the Prime Meridian and north of the Equator for monocrystalline panels. The same results are seen for polycrystalline panels but in the opposite direction with respect to the Prime Meridian. Consistently small coefficients corresponding to longitude's individual effect suggest a relatively insignificant impact. Additional data will enable increased specificity on this point. It is worth noting that latitude's effect is not fully known due the lack of test sites in the Southern Hemisphere.

For all cases, power output decreased with increasing humidity and increased with increasing temperature. Interaction between temperature and humidity always resulted in increased power. These results may confirm that during the presence of increased overall solar radiation, ambient temperature was increased and humidity aided in the absorption of diffuse radiation. The interaction also shows that higher humidity mitigates the effects of lower amounts of direct radiation and temperature, supporting the results obtained in the experiments conducted by the Brusaws (see Chapter II). This interaction was significant in nearly all location-specific models, in some cases having a greater effect than ambient temperature alone. Humidity's effect, without any interaction, was much less impactful or not included at all. This further confirms the important link between the two factors and the importance of their inclusion in the study.

Surface Variance Test

Identical test systems operated at Tec^Edge Works (TEW) in Dayton, Ohio, on different surface types for the purpose of identifying additional factors possibly impacting regression model fit. Results of the test, provided in Figure 30, show a statistically significant difference between the two-sample means. Closer inspection of the difference in means with a range of zero to 20 watts, indicates average energy production is approximately two watts higher on the ground than on roofs during the months of November and December. Distribution of temperature and humidity among the two surface types, displayed in Figure 31, reveal a lower average temperature and humidity measured by the roof system compared to the ground systems. Initially, it may seem that elevation has an effect on power output. However, previous results consistently linked higher humidity and lower temperatures with less power produced. This explains why the rooftop system produced less power. The higher temperatures on the ground may be attributed to shielding of wind by the building adjacent to the test site. The roof system is not shielded from wind in any direction and thus more susceptible to wind chill effects. Regardless, inclusion of elevation as a potential predictor would be simple and provide another way of discovering or ruling out additional model effects.

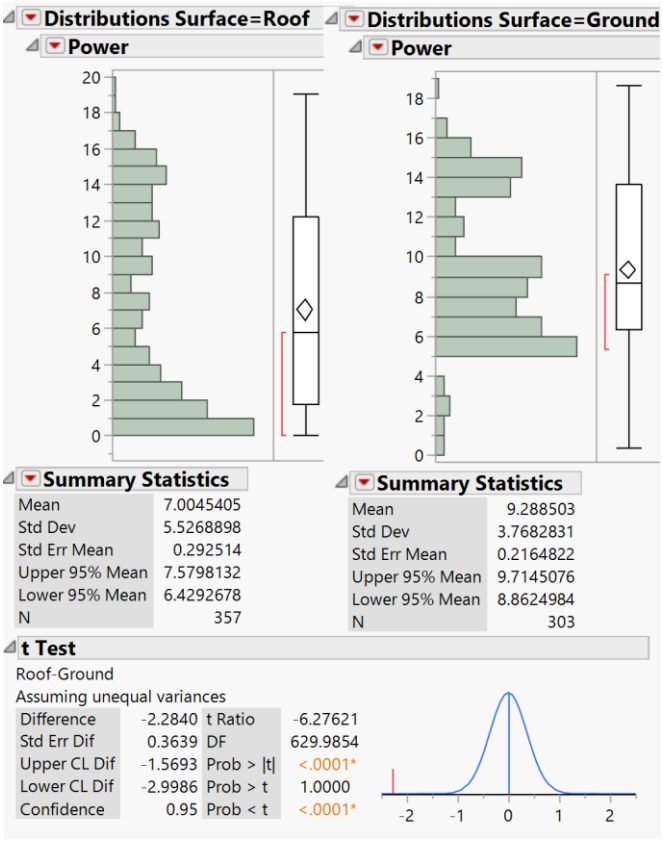

Figure 30. two-sample t-test comparing ground and roof system output

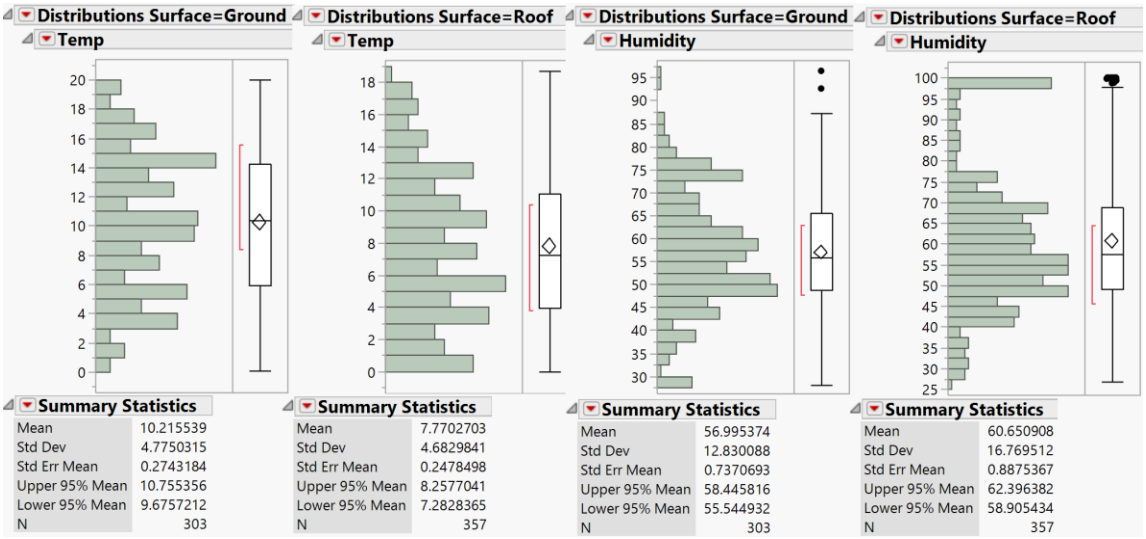

Figure 31. temperature and humidity distributions by surface type

V. CONCLUSIONS AND RECOMMENDATIONS

The following sections summarize the analysis from the previous chapter and allow future researchers and decision-makers a point of reference to continue research into global horizontal photovoltaic (PV) panel performance. The primary purpose of this research aimed to impact a U.S. Air Force effort to bolster energy resilience and satisfy clean energy mandates by the U.S. government. This is partly achieved by providing decision-makers with technological solutions involving renewable sources such as wind, hydro, solar, and other power sources. Solar power has a great amount of untapped potential for energy production that can be harnessed through judicious use of technological innovations such as PV. This study confirms a link between temperature and humidity with power output at most locations, though the link diminishes at some. Key insights were obtained from this study into horizonal PV and opportunities to bolster current and future research were identified.

Key Points

The current data is insufficient to model power production globally or by major climate type. Individual locations have some highly predictive models while others require more predictors to gain any kind of predictive value. In general, models pertaining to monocrystalline PV were more predictive, meaning variance in power output was explained by the given factors slightly more than the polycrystalline. Current models do not provide enough information to justify expenditure of funds on polycrystalline technology. Therefore, any forecasting effort would be better served

using monocrystalline PV for specific installations (intra-state or local area) in which accuracy was greatest.

These data show that one or more interacting predictor variables are missing from the models. This is shown by the significance of latitude and longitude and their effects on global and climate models. They indicate their encapsulation of environmental conditions that change in conjunction with global position. Air mass, elevation, rainfall, wind speed, and other factors may interact with or have significantly greater independent effects than temperature and humidity on their own. Current data is mainly composed of autumn months with partial summer and winter seasonal data. A full year of measurements, per the study's design, will reveal the full extent to which these factors interact and affect power output covering all seasonal conditions. Now that test locations are well-established and site-monitors are familiar with the test systems and expectations, subsequent research will be able to garner data from a larger number of test sites and increase data quantity and quality. Finally, continuation of this line of research would benefit from modifications to the current study whether they be part of this initial year of data gathering or subsequent years of research.

Recommendations for Future Research

One predictor variable that is likely to explain variance in power output is the amount of periodic direct, diffuse, and reflected solar radiation. As of this writing, real-time solar irradiance data is not being gathered by test sites and the latest datasets available that provide this information are dated June 2005 from the Atmospheric Science Data Center at the National Aeronautics and Space Administration (NASA). However,

cloud cover and other conditions that affect penetration of solar rays can change rapidly within short time periods. Therefore, a method should be devised for measuring the amount of direct, diffuse, and reflected solar radiation in immediate test areas. This can be partly accomplished through the use of a pyranometer, such as those incorporated in GMX101 Solar Radiation Sensors, pictured in Figure 41. Resulting data, combined with a full year of ambient temperature and humidity readings for both panel types, are expected to provide a wealth of explanatory information regarding the effects of humidity and temperature on horizontal silicon-based PV panels in varying lighting conditions. In addition, improvements to data quality and inclusion of additional variables can be performed at researcher discretion to uncover additional effects and refine model fits.

Figure 32. GMX101 Solar Radiation Sensor (Omni Instruments, 2018)

Reliability of acquired data can be improved by ensuring uniform guidance to test site monitors describing proper test system placement and periodic maintenance. Varying site-specific conditions can be accounted for by requesting that each monitor submit photographs capturing a 360-degree view of their respective site. Trees and other

obstructions causing periodic shading of the panels can be taken into account. Additional variables can also be considered for inclusion such as climate types narrowed beyond the five Köppen climate types, periodic (daily or hourly) rain or snow fall, presence of fog or smog, site elevation above sea level, surface type, etc. Finally, incorporating enough predictors to hone regression models to an accuracy that is satisfactory should prompt an analysis using time-series or other forecasting technique that enables decision-making based on expected power production (per month or season).

Incorporating this additional level of effort would require staffing and funding sources that may be beyond the scope of a single researcher at AFIT to conduct. However, this study was a team effort involving engineers and graduate students from multiple departments coming together to design and manufacture the test systems used during the research. Funding was appropriated by multiple stakeholders interested in the possibility of utilizing horizontal PV for energy applications. Similar collaborative efforts could and should be made to bolster the current study with additional funding, equipment, and expertise that will greatly improve the validity of performance models and ultimately the ability of military leadership to make informed decisions toward using this technology to supplement their energy portfolios.

Appendix – Performance Model Analyses

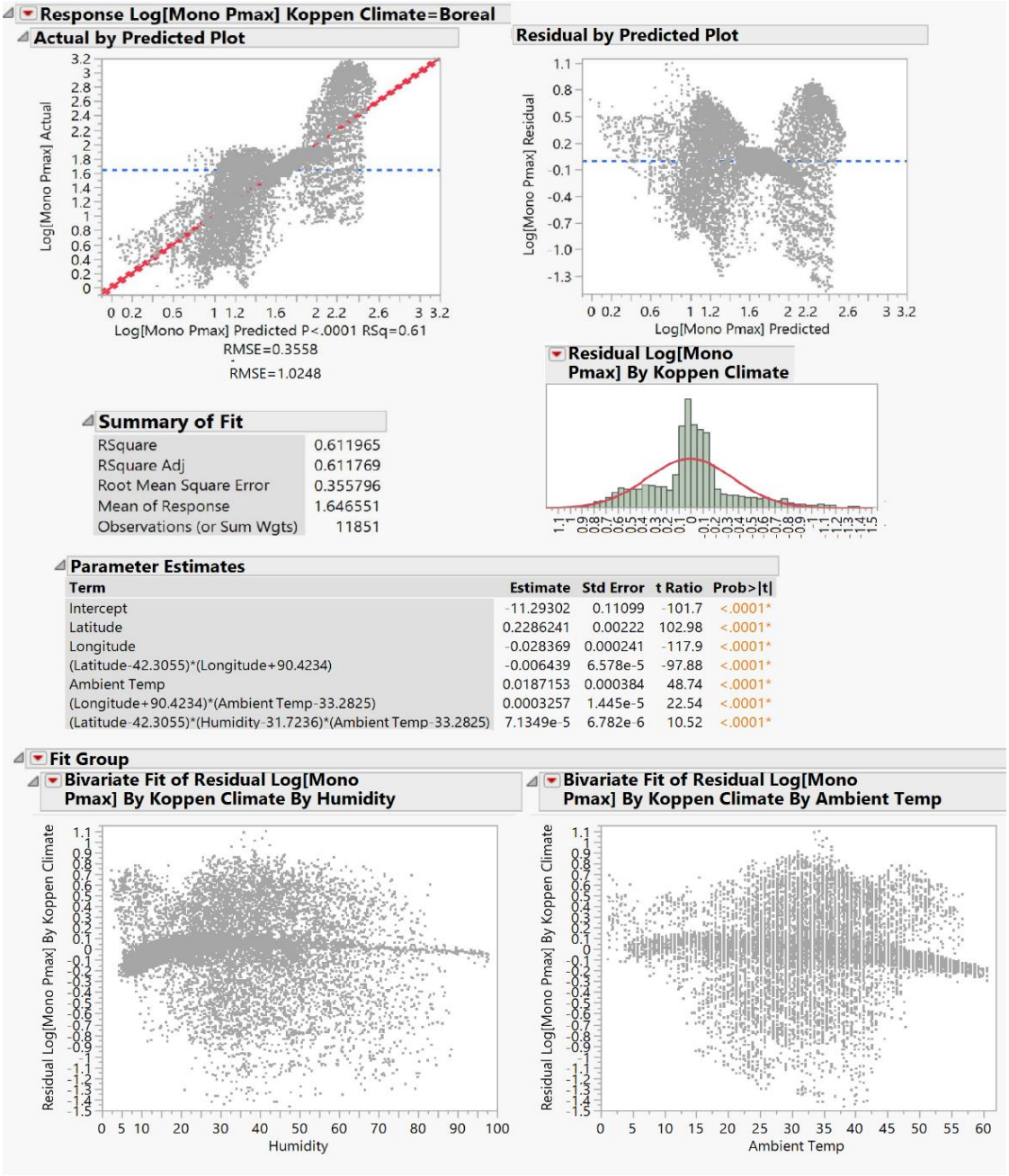

Figure 33. Monocrystalline model and diagnostics for boreal climate

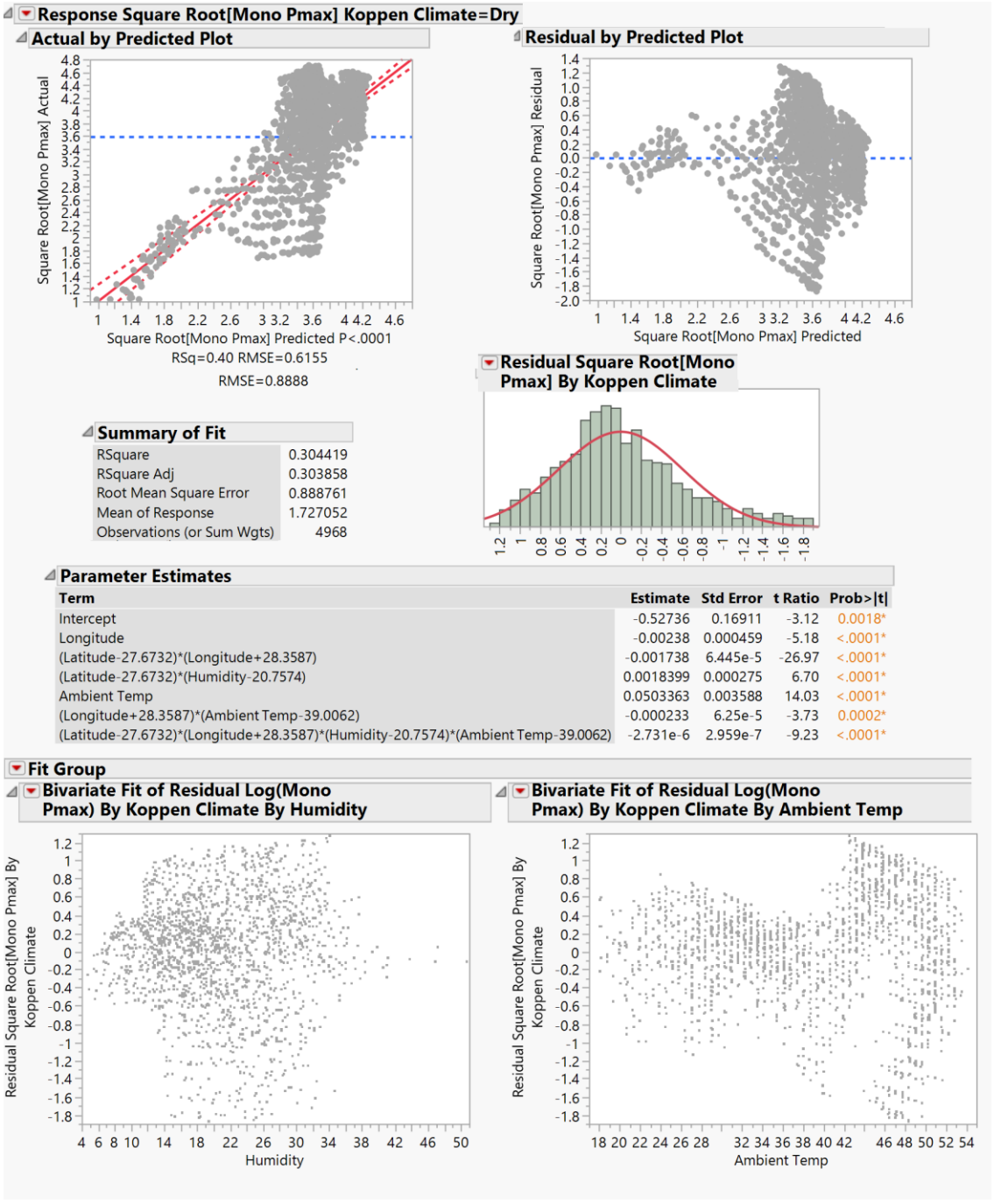

Figure 34. Monocrystalline model and diagnostics for dry climate

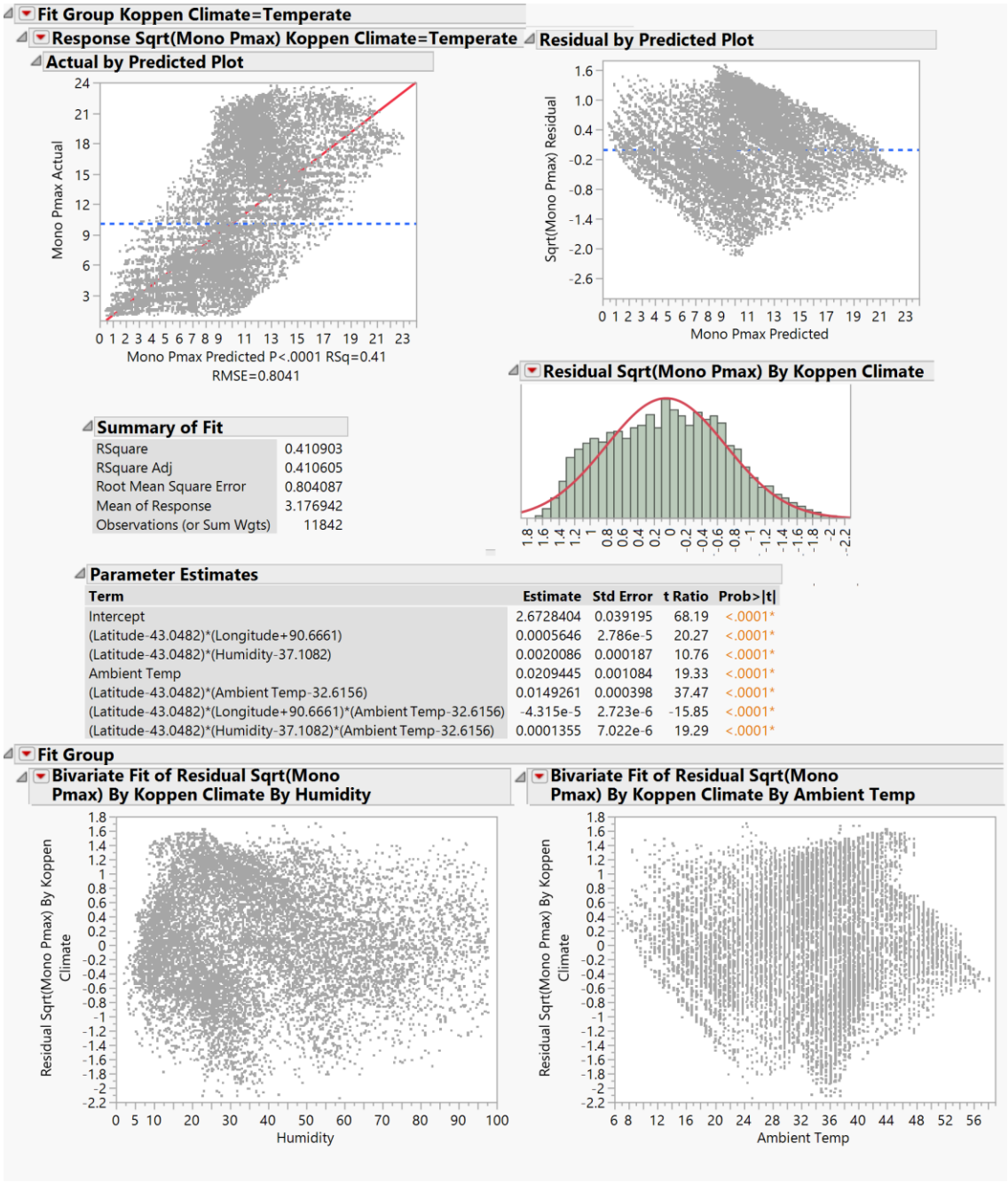

Figure 35. Monocrystalline model and diagnostics for temperate climate

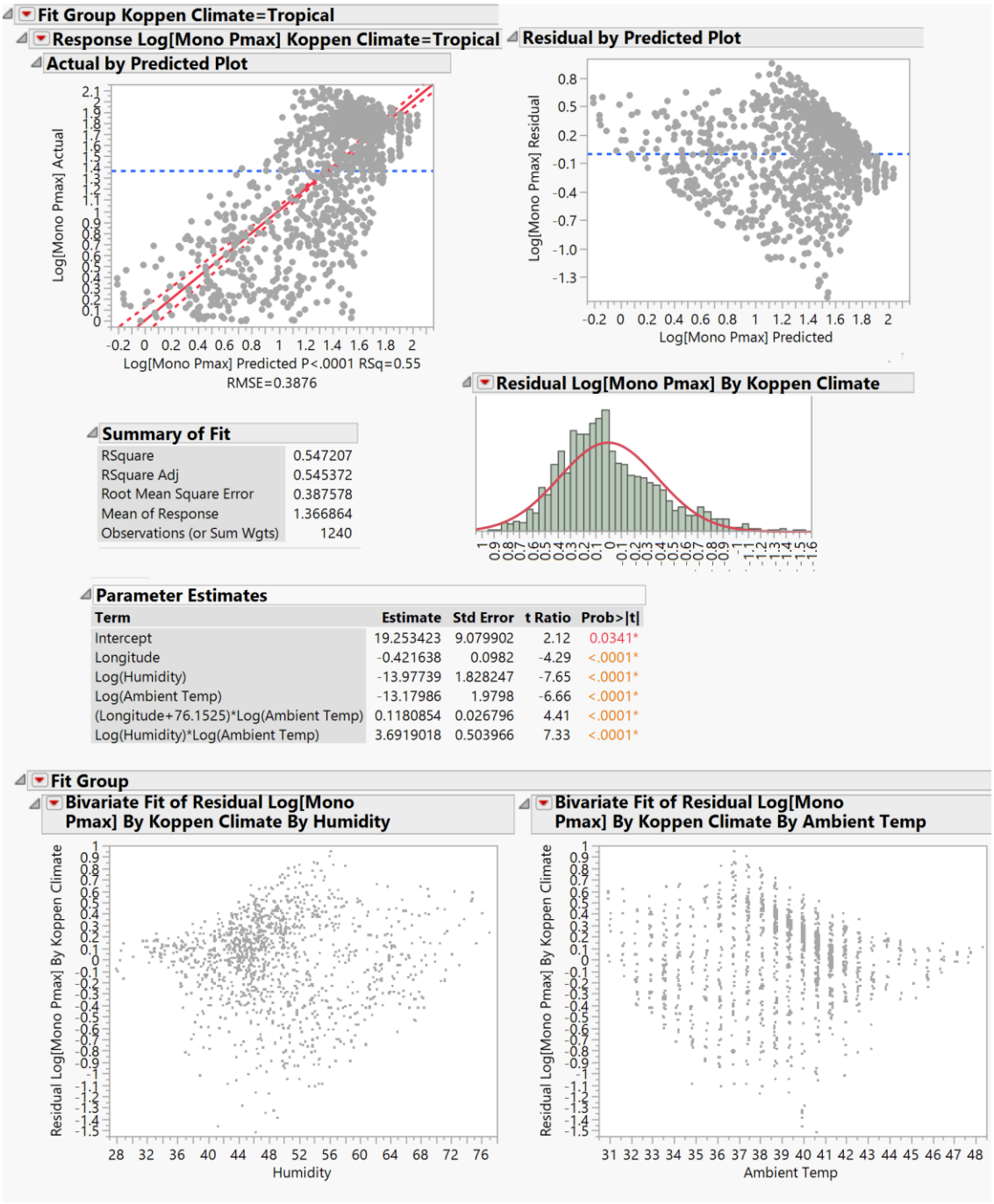

Figure 36. Monocrystalline model and diagnostics for tropical climate

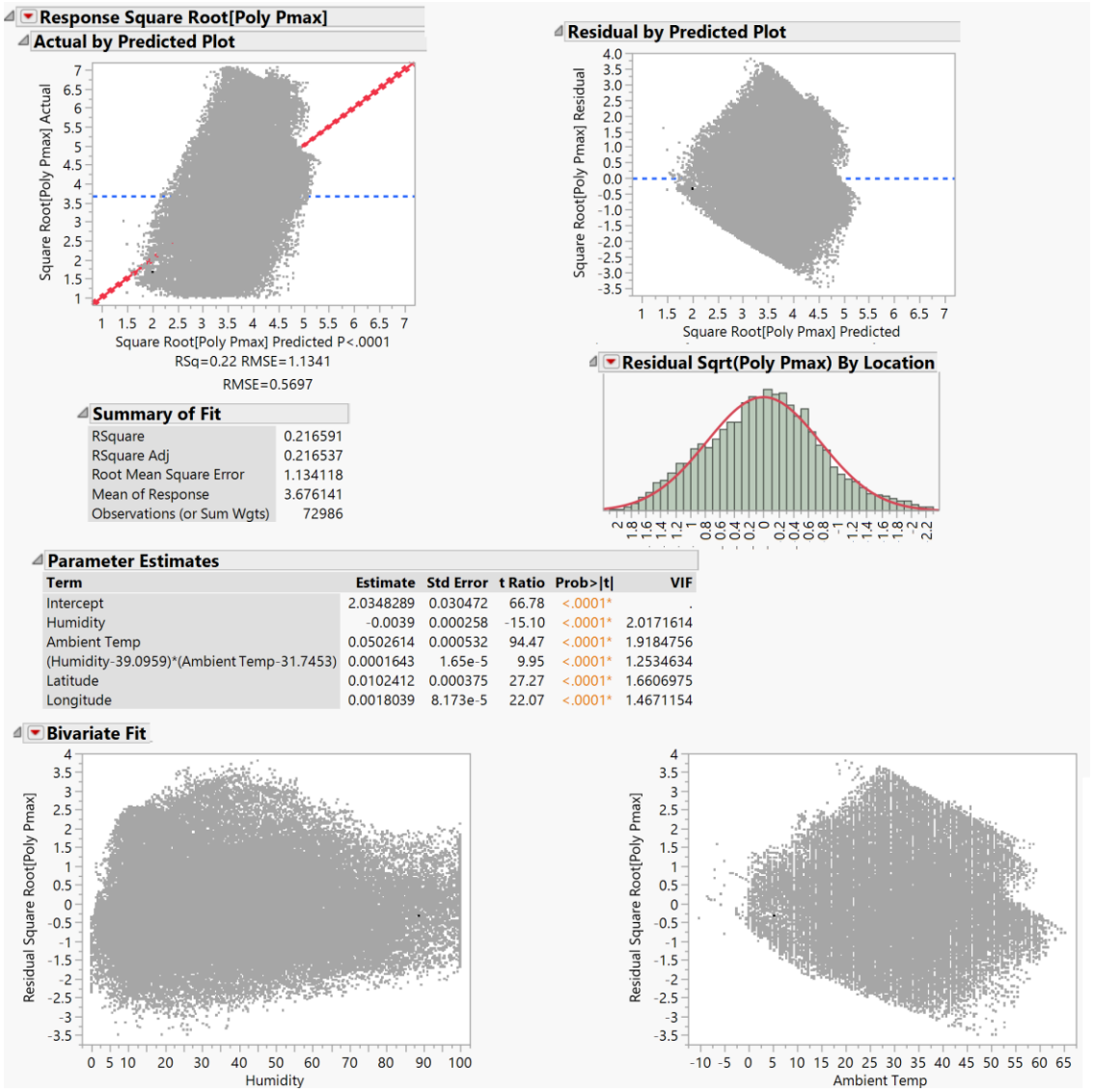

Figure 37. Global polycrystalline model and diagnostics

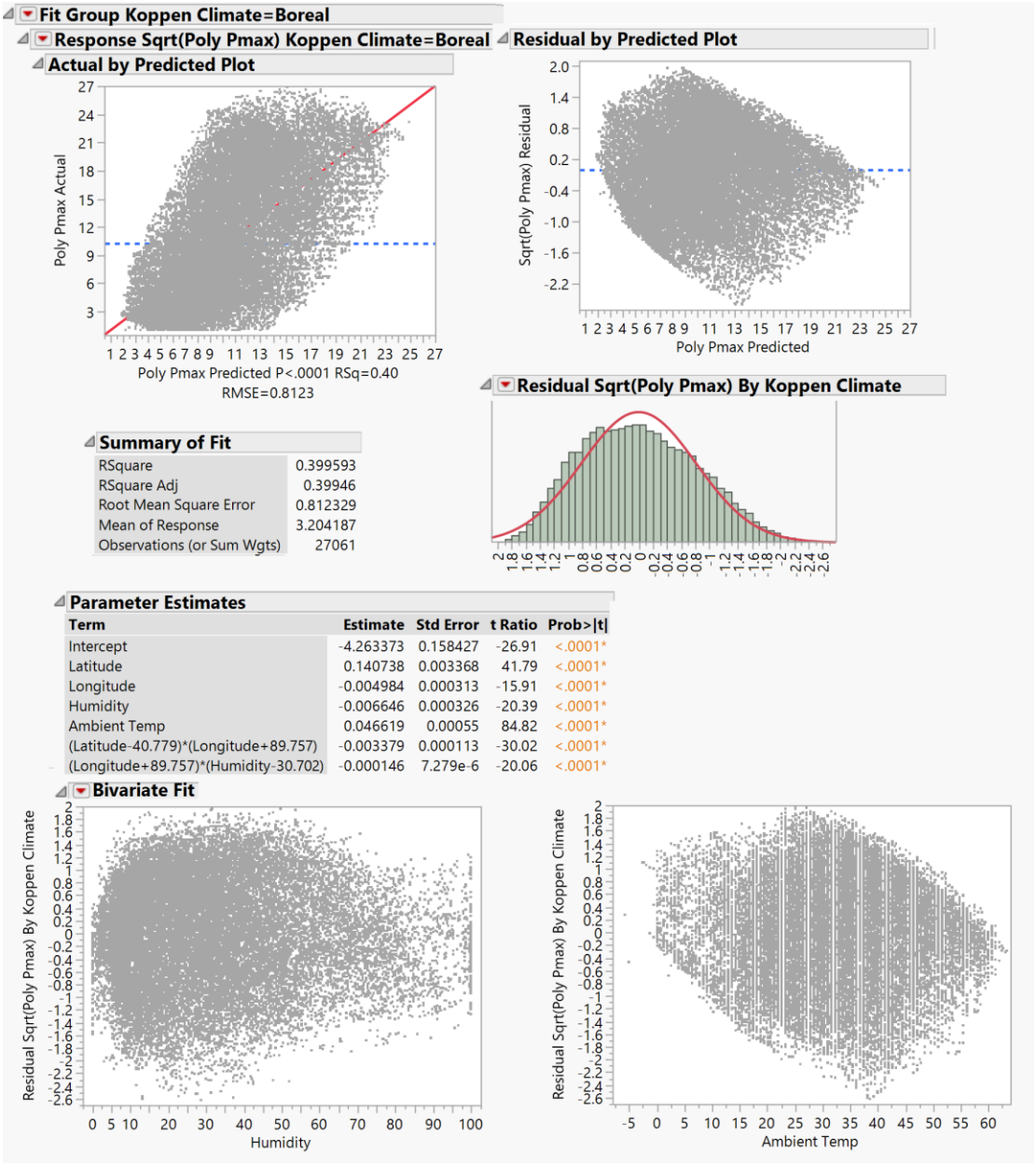

Figure 38. Polycrystalline model and diagnostics for boreal climate

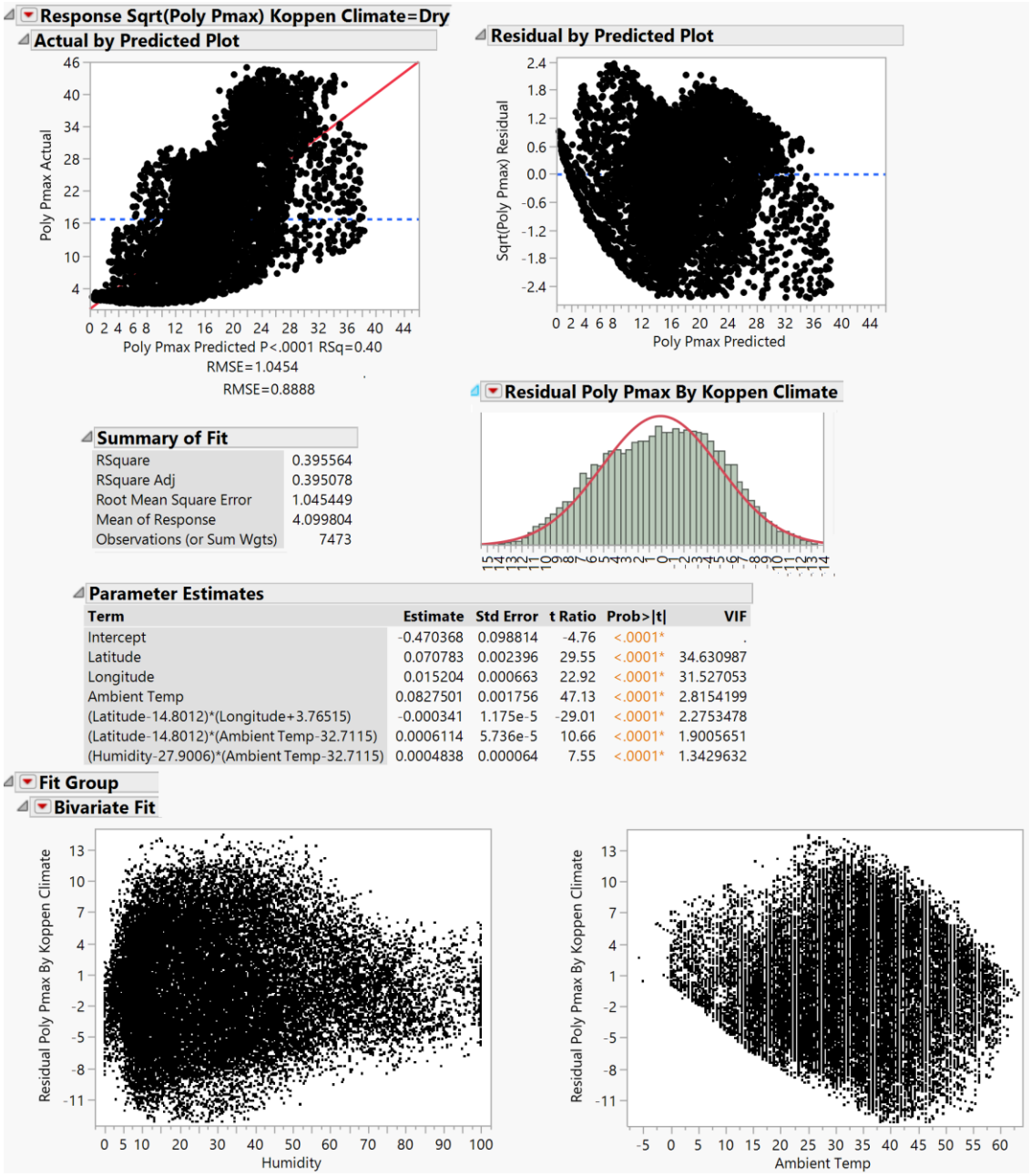

Figure 39. Polycrystalline model and diagnostics for dry climate

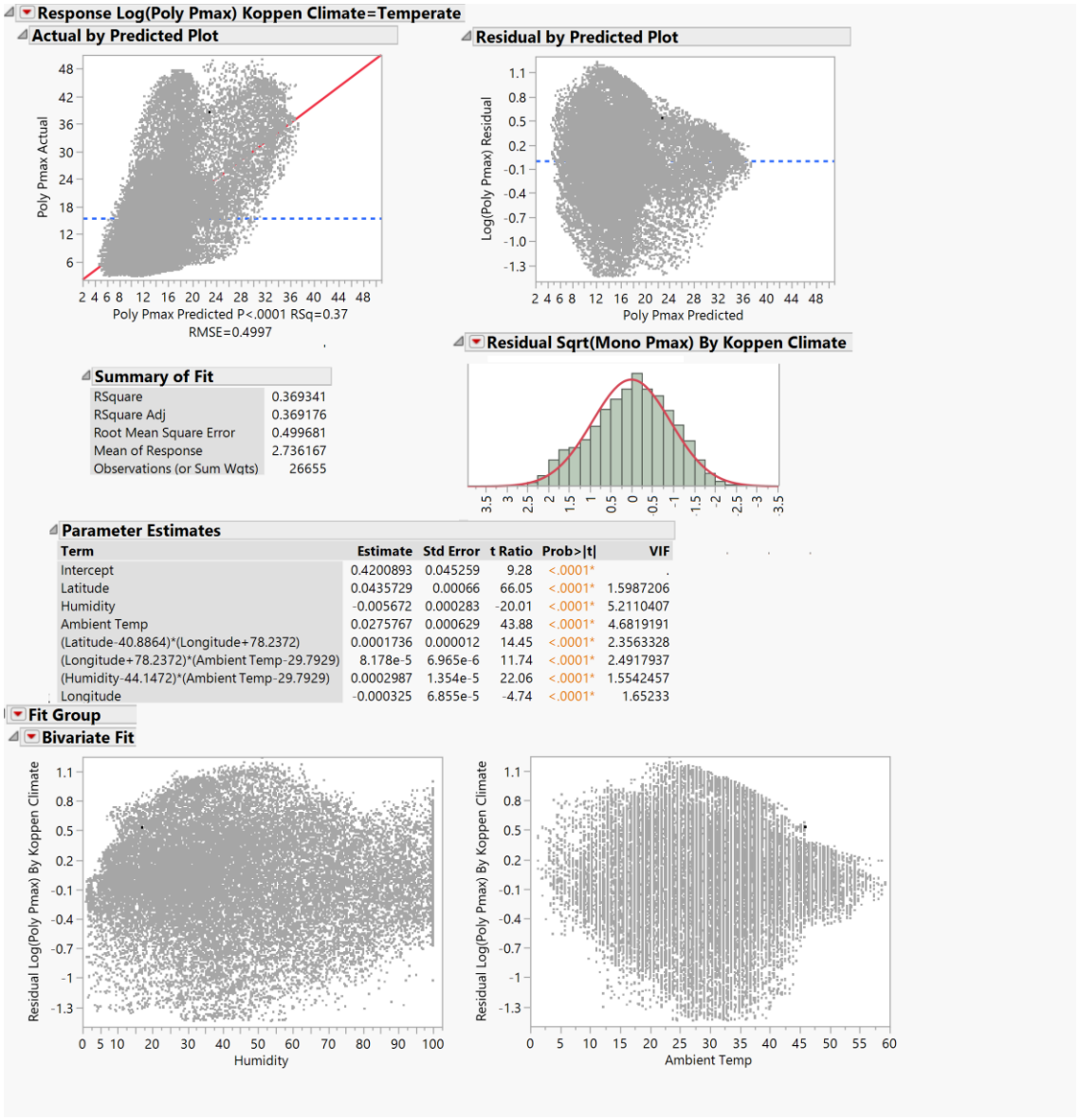

Figure 40. Polycrystalline model and diagnostics for temperate climate

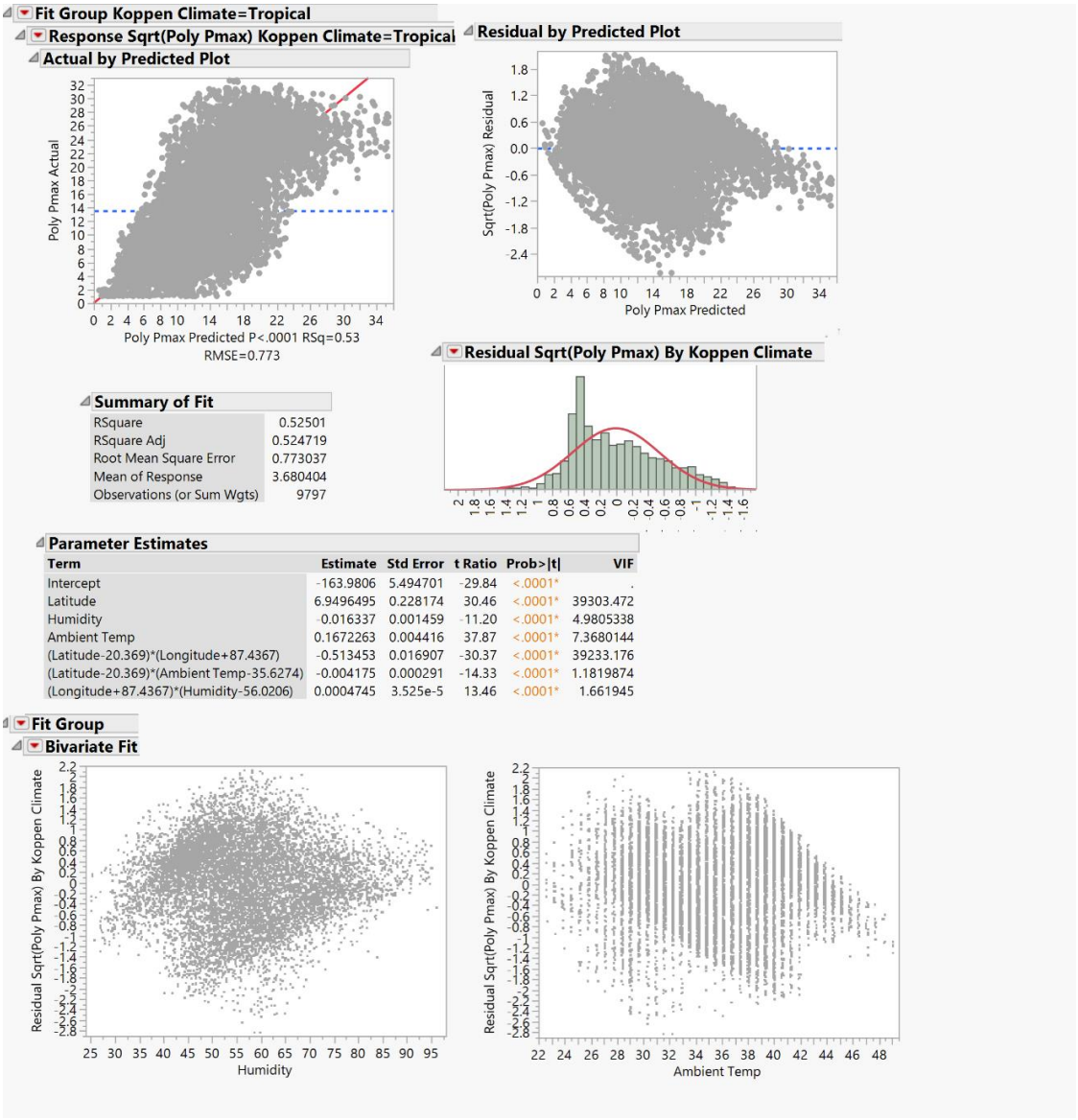

Figure 41. Polycrystalline model and diagnostics for tropical climate

References

Astronomical Applications Department. (2016, Jun 1). *Sun or Moon Rise/Set Table for One Year*. Retrieved from Astronomical Applications Department of the U.S. Naval Observatory: http://aa.usno.navy.mil/data/docs/RS_OneYear.php

AA Portable Power Corp. (2017). *SLA Battery:Regulated Sealed Lead Acid Battery 12V 12Ah with Overcharge and Overdischarge Protection*. Retrieved from BatterySpace.com: http://www.batteryspace.com/regulatedleadacidbattery12v12ahwithoverchargeandoverdischargeprotection.aspx

Airforce Civil Engineer Center (AFCEC) Energy Directorate. (2014). *Building the Air Force Renewable Energy Portfolio - Meeting the 2015 Energy Goals.* AFCEC.

Beck, C., Grieser, J., & Rubel, F. (2005). Characterizing Global Climate Change by means of Koppen Climate Classification. *ResearchGate*, 13.

Brusaw, E., & Brusaw, J. (2016). *Research & Findings: Phase IIB Research*. Retrieved from Solar Roadways: http://www.solarroadways.com/Research/Funding#

Buro, K. (2018). *Department of Mathematics & Statistics*. Retrieved from MacEwan University: https://academic.macewan.ca/burok/Stat378/notes/remedies.pdf

Cameron, C. P., Boyson, W. E., & Riley, D. M. (2008). *Comparison of PV System Performance-Model Predictions with Measured PV System Performance.* Sandia National Laboratories.

De Soto, W., & Klein, S. (2005). Improvement and Validation of a Model for Photovoltaic Array Performance. *Solar Energy Laboratory, University of Wisconsin*.

Fanney, A. H., Dougherty, B. P., & Davis, M. W. (2009). Comparison of Predicted to Measured Photovoltaic Module Performance. *Journal of Solar Energy Engineering*, vol. 131.

Fingas, J. (2016, Oct 2). *Solar road tiles get their first public test*. Retrieved from 2018 Oath Tech Network Aol Tech: https://www.engadget.com/2016/10/02/solar-roadways-public-test/

Ghasemi, A., & Zahediasl, S. (2012, Apr 20). *Normality Tests for Statistical Analysis: A Guide for Non-Statisticians*. Retrieved from National Center for Biotechnology Information: https://www.ncbi.nlm.nih.gov/pmc/articles/PMC3693611/

Koussa, M., Haddadi, M., Saheb, D., Malek, A., & Hadji, S. (2012). Sun tracker systems effects on flat plate photovoltaic PV systems performance for different sky states: A case of an arid. *Elsevier Ltd. Selecti*.

Landau, C. R. (2015). *Optimal Tile of Solar Panels*. Retrieved from http://www.solarpaneltilt.com/

Laube, P. (2018). *Fundamentals: Doping: n- and p-semiconductors*. Retrieved from Semiconductor Technology from A to Z: https://www.halbleiter.org/en/fundamentals/doping/

Maehlum, M. A. (2015, April 6). *Best Thin Film Solar Panels – Amorphous, Cadmium Telluride or CIGS?* Retrieved from Energy Informative: http://energyinformative.org/best-thin-film-solar-panels-amorphous-cadmium-telluride-cigs/

Maehlum, M. A. (2017, Aug 5). *Which Solar Panel Type is Best? Mono- vs. Polycrystalline vs. Thin Film*. Retrieved from Energy Informative: http://energyinformative.org/best-solar-panel-monocrystalline-polycrystalline-thin-film/

Maksimovic, M., & Vujovic, V. (2014). Raspberry Pi as a Wireless Sensor node: Performances and constraints. *ResearchGate*, 7.

Mekhile, S., Saidur, R., & Kamalisarvestani, M. (2012). Effect of Dust, Humidity, and Air Velocity on Efficiency of Photovoltaic Cells. *Renewable and Sustainable Energy Reviews*, no. 16, pp. 2920-2925.

Meserve, J. (2007, September 27). *Mouse Click Could Plunch City into Darkness, Experts Say*. Retrieved from CNN: http://www.cnn.com/2007/US/09/27/power.at.risk/index.html#cnnSTCText

Nagangast, C., Hendrickson, C., & Matthew, H. S. (2013). Variations in Photovoltaic Performance Due to Climate and Low-Slope Roof Choice. *Energy and Buildings*, no. 64, pp. 493-502.

National Aeronautics and Space Administration. (2018). *NASA Surface meteorology and Solar Energy: Global Data Sets*. Retrieved from Atmospheric Science Data Center: https://eosweb.larc.nasa.gov/cgi-bin/sse/global.cgi

National Energy Foundation. (2017). *Types of Photovoltaic (PV) Cells*. Retrieved from http://www.nef.org.uk/knowledge-hub/solar-energy/types-of-photovoltaic-pv-cells

Nussbaum, J. H. (2017). *Analyzing the Viability of Photovoltaic Pavement Systems: Quantifying Climate Impacts on Potential Power and the Risks of Implementation.* Wright-Patterson Air Force Base: Air Force Intitute of Technology.

Office of Energy Efficiency & Renewable Energy. (2013, Aug 16). *Solar Photovoltaic Technology Basics*. Retrieved from U.S. Department of Energy: https://energy.gov/eere/solar/articles/solar-photovoltaic-technology-basics

Office of Energy Efficiency & Renewable Energy. (2018). *Achieving 30% Renewable Electricity Use by 2025*. Retrieved from U.S. Department of Energy: https://energy.gov/eere/femp/achieving-30-renewable-electricity-use-2025

Omni Instruments. (2018). *GMX101 Solar Radiation Sensor*. Retrieved from http://www.omniinstruments.co.uk/weather-stations-and-instruments/pyranometers-solar-irradiance/gmx101-weather-station.html

Pew Project on National Security, Energy, and Climate, Clean Energy Initiative. (2014, February). *Military's Largest Solar Array Opens at Davis-Monthan Air Force Base.* Retrieved from The PEW Charitable Trusts: http://www.pewtrusts.org/en/research-and-analysis/analysis/2014/02/28/militarys-largest-solar-array-opens-at-davismonthan-air-force-base

Rock Seven. (2014). *RockBlock MK2*. Retrieved from http://www.rock7mobile.com/products-rockblock

Rosell, J. I., & Ibanez, M. (2006). Modelling Power Output in Photovoltaic Modules for Outdoor Operating Conditions. *Energy Conversion and Mangement*, 2424-2430.

Skoplaki, E., & Palyvos, J. A. (2008). On the Temperature Dependence of Photovoltaic Module Electrical Performance: A Review of Efficiency/Power Correlations. *Solar Energy*, no. 83, pp. 614-624.

Statistics How To. (2018). *Regression Analysis: Step by Step Articles, Videos, Simple Definitions*. Retrieved from http://www.statisticshowto.com/probability-and-statistics/regression-analysis/

Statistics Solutions. (2018). *Assumptions of Multiple Linear Regression*. Retrieved from http://www.statisticssolutions.com/assumptions-of-multiple-linear-regression/

Statistics Solutions. (2018). *Multiple Linear Regression*. Retrieved from http://www.statisticssolutions.com/multiple-lr/

Sukamongkol, Y., Chunpaibulpatana, S., & Ongsakul, W. (2001). *"A Simulation Model for Predicting the Performance of a Solar Photovoltaic System with Alternating Current Loads.* Sirindhorn International Institute of Technology, Asian Institute of Technology.

TechyChaps. (2017, September 2). Retrieved from How do Solar Panels work and Generate Electricity??: https://www.techychaps.com/solar-panels-work/

U.S. Air Force. (2014, July). *Nellis AFB to Add Second Large Solar Plan.* Retrieved from Official United States Air Force Website: http://www.af.mil/News/Article-Display/Article/486227/nellis-afb-to-add-second-large-solar-plant/

U.S. Air Force. (2017, Jan 6). *Energy Flight Plan.* Retrieved from U.S. Air Force Civil Engineer Center: http://www.safie.hq.af.mil/Portals/78/AFEnergyFlightPlan2017.pdf?ver=2017-01-13-133958-503

US Congress. (2010). *National Defense Authorization Act (NDAA).* Retrieved from Defense Technical Information Center: http://www.dtic.mil/congressional_budget/pdfs/FY2010_pdfs/AUTH_CONF_111-288.pdf

US Department of Defense. (2016, February 16). *Fiscal Year 2017 Budget Fact Sheet, 2016.* Retrieved from United States Department of Defense (DoD): https://www.defense.gov/Portals/1/features/2016/0216_budget/docs/2-4-16_Consolidated_DoD_FY17_Budget_Fact_Sheet.pdf

USAF. (2013). *AFD-130325-124 U.S. Air Force Energy Strategic Plan.* U.S. Department of Defense.

Volz, D. (2017, May 12). *Global cyber attack fuels concern about U.S. vulnerability disclosures*. Retrieved from Reuters: https://www.reuters.com/article/us-britain-security-hospitals-nsa/global-cyber-attack-fuels-concern-about-u-s-vulnerability-disclosures-idUSKBN1882ZF

WebElements. (2018). *Silicon: the essentials*. Retrieved from https://www.webelements.com/silicon/

Wei , Z., Yang, H., & Fang, Z. (2007). *A Novel Model for Photovoltaic Array Performance Prediction.* Hong Kong: The Hong Kong Polytechnic University, Shandong University of Architecture.

REPORT DOCUMENTATION PAGE

Form Approved
OMB No. 0704-0188

PLEASE DO NOT RETURN YOUR FORM TO THE ABOVE ADDRESS.

1. REPORT DATE *(DD-MM-YYYY)*	2. REPORT TYPE	3. DATES COVERED *(From - To)*
22-03-2018	Master's Thesis	Oct 2016 - Mar 2018

4. TITLE AND SUBTITLE

ANALYSIS OF TEMPERATURE AND HUMIDITY EFFECTS ON HORIZONTAL PHOTOVOLTAIC PANELS

5a. CONTRACT NUMBER

5b. GRANT NUMBER

5c. PROGRAM ELEMENT NUMBER

6. AUTHOR(S)

Booker, Corey J, Capt

5d. PROJECT NUMBER

5e. TASK NUMBER

5f. WORK UNIT NUMBER

7. PERFORMING ORGANIZATION NAME(S) AND ADDRESS(ES)

Air Force Institute of Technology
Graduate School of Engineering and Management (AFIT/ENV)
2950 Hobson Way
Wright-Patterson AFB OH 45433-7765

8. PERFORMING ORGANIZATION REPORT NUMBER

AFIT-ENV-MS-18-M-180

9. SPONSORING/MONITORING AGENCY NAME(S) AND ADDRESS(ES)

Mr Robert T. Bossert, Jr.
National Guard Bureau/Operations Division (NGB/A4OC)
3500 Fetchet Avenue
Joint Base Andrews, MD 20762
(701) 857-4350 Robert.t.bossert.civ@mail.mil

10. SPONSOR/MONITOR'S ACRONYM(S)

11. SPONSOR/MONITOR'S REPORT NUMBER(S)

12. DISTRIBUTION/AVAILABILITY STATEMENT

Distribution Statement A: Approved for Public Release; Distribution Unlimited

13. SUPPLEMENTARY NOTES

This work is declared a work of the U.S. Government and is not subject to copyright protection in the United States.

14. ABSTRACT

The USAF seeks to address power grid vulnerability/bolter energy resilience through the use of renewable energy. AFIT engineers designed and manufactured controls to monitor power output from the most widely-used silicon-based solar cells at 38 testing locations around the globe including majority of climate types. Multivariate regression analysis established a statistical relationship between photovoltaic power, ambient temperature, and humidity for monocrystalline and polycrystalline photovoltaics. Models first characterized power globally then by specific climate type with general inaccuracy. Location-specific models are provided with varying accuracy, allowing some locations to predict energy output/make decisions regarding energy projects. Additional predictor variables are required to hone model accuracy. Recommendations are made that modify the current study to increase data quality and ensure validity/accuracy of regression models/future ability to forecast power production for use by decision-makers. A full year of measurements combined with proposed modifications will demonstrate feasibility of utilizing horizontal photovoltaic technology.

15. SUBJECT TERMS

Photovoltaic, humidity, temperature, renewable energy

16. SECURITY CLASSIFICATION OF:			17. LIMITATION OF ABSTRACT	18. NUMBER OF PAGES	19a. NAME OF RESPONSIBLE PERSON
a. REPORT	b. ABSTRACT	c. THIS PAGE			Dr. Alfred E. Thal, Jr., AFIT/ENV
U	U	U	UU	92	19b. TELEPHONE NUMBER *(Include area code)* (937) 785-3636 x7401 alfred.thal@afit.edu

Reset